Cold-water corals as archives of seawater Zn and Cu isotopes

Susan H. Little[1,2*], David J. Wilson[1], Mark Rehkämper[2], Jess F. Adkins[3], Laura F. Robinson[4], Tina van de Flierdt[2]

1. Department of Earth Sciences, University College London, Gower Place, London, WC1E 6BS, UK.

*susan.little@ucl.ac.uk

2. Department of Earth Science and Engineering, Royal School of Mines, Imperial College London, London, SW7 2BP, UK

3. Division of Geological and Planetary Sciences, California Institute of Technology, Pasadena, CA 91125, US.

4. School of Earth Sciences, University of Bristol, Bristol, BS8 1RJ, UK.

Resubmission deadline: 23 April 2021

Invited submission to *Chemical Geology*

Abstract

Traditional carbonate sedimentary archives have proven challenging to exploit for Zn and Cu isotopes, due to the high concentrations of trace metals in potential contaminants (e.g., Fe-Mn coatings) and their low concentrations in carbonate. Here, we present the first dataset of $\delta^{66}Zn_{JMC\text{-}Lyon}$ and $\delta^{65}Cu_{SRM\ 976}$ values for cold-water corals and address their potential as a seawater archive. Extensive cleaning experiments carried out on two corals with well-developed Fe-Mn rich coatings demonstrate that thorough physical and chemical cleaning can effectively remove detrital and authigenic contaminants. Next, we present metal/Ca ratios and $\delta^{66}Zn$ and $\delta^{65}Cu$ values for a geographically diverse sample set of Holocene age cold-water corals. Comparing cold-water coral $\delta^{66}Zn$ values to estimated ambient seawater $\delta^{66}Zn$ values (where $\Delta^{66}Zn_{coral\text{-}sw} = \delta^{66}Zn_{coral} - \delta^{66}Zn_{seawater}$), we find $\Delta^{66}Zn_{coral\text{-}sw} = +0.03 \pm 0.17‰$ (1SD, n = 20). Hence, to a first order, cold-water corals record seawater Zn isotope compositions without fractionation. The average Holocene coral Cu isotope composition is $+0.59 \pm 0.23‰$ (1SD, n = 15), similar to the mean of published deep seawater $\delta^{65}Cu$ values at $+0.66 \pm 0.09‰$, but with considerable variability. Finally, $\delta^{66}Zn$ and $\delta^{65}Cu$ data are presented for a small subset of four glacial-age corals. These values overlap with the respective Holocene coral datasets, hinting at limited glacial-interglacial changes in oceanic Zn and Cu cycling.

1. Introduction

Zinc (Zn) and copper (Cu) are bioessential trace metals with isotopic systems that are emerging as promising tracers of past ocean nutrient and redox cycling. To date, reliable archives for past seawater Zn and Cu isotopes have been lacking, because both metals are present at low concentrations in carbonate and opal, but at high concentrations in potential contaminating material, such as detrital or authigenic (e.g., Fe-Mn oxide) phases (Boyle, 1981; Shen and Boyle, 1988; Pichat et al., 2003; Andersen et al., 2011; Hendry and Andersen, 2013). Zinc isotopes have previously been applied in Pleistocene to ancient marine sediments, typically using bulk carbonate leachates in an attempt to side-step the contamination problem (Pichat et al., 2003; Kunzmann et al., 2013; John et al., 2017; Liu et al., 2017; Sweere et al., 2018). We propose that cold-water coral skeletons provide an exciting new possibility for a seawater Zn and Cu isotope archive. Their global distribution, combined with an ability to obtain precise ages for individual specimens, gives corals distinct advantages over more traditional palaeoclimate archives (e.g., Robinson et al., 2014), potentially enabling reconstructions of ocean chemistry on centennial or even shorter timescales (e.g., Wilson et al., 2014; Chen et al., 2015). In addition, their large size confers a particular advantage for analysing trace metal isotopes, because it should enable rigorous cleaning to remove surficial contaminant phases, while still providing sufficient quantities of Zn and Cu for isotope analysis.

Zinc has a classic nutrient-type distribution in the modern ocean, reflecting a combination of biological cycling and the physical ocean circulation (Bruland, 1980; Vance et al., 2017; Middag et al., 2019). Away from local sedimentary sources and hydrothermal vents, the deep ocean is isotopically homogeneous, at about +0.45‰ (δ^{66}Zn relative to JMC-Lyon), while the upper ocean exhibits considerable variability, ranging from -1.1 to +1.2‰ (Conway and John, 2014; Zhao et al., 2014; Samanta et al., 2017; John et al., 2018; Wang et al., 2018; Vance et al., 2019; Liao et al., 2020; Sieber et al., 2020). The origin of this variability remains a subject of debate. Biological uptake in the Southern Ocean is associated with no isotopic fractionation or with small deviations towards isotopically heavy Zn in the residual dissolved phase (Zhao et al., 2014; Wang et al., 2018; Sieber et al., 2020), consistent with evidence for limited isotopic fractionation on uptake by diatoms (John et al., 2007; Köbberich and Vance,

2017). However, marked deviations towards isotopically light sub-surface Zn are observed in the water column elsewhere (e.g., Conway and John, 2014). Explanations proposed for this phenomenon include shallow remineralisation of isotopically light organic matter (Samanta et al., 2017; Vance et al., 2019), removal by scavenging of isotopically heavy Zn (Conway and John, 2014; John and Conway, 2014; Weber et al., 2018; Liao et al., 2020), and/or inputs from an isotopically light external Zn source (Lemaitre et al., 2020; Liao et al., 2020).

Dissolved Cu concentrations in the ocean increase approximately linearly with depth (Boyle et al., 1977; Bruland, 1980). This profile shape has been described as "hybrid-type" and attributed to a combination of biological uptake and scavenging (Bruland et al., 2013). However, the respective roles of (a) reversible scavenging in the water column and (b) irreversible scavenging followed by benthic sedimentary input remain to be fully deconvolved (Boyle et al., 1977; Little et al., 2013, 2018; Roshan and Wu, 2015; Richon and Tagliabue, 2019). A key feature of Cu (and, to a lesser extent, Zn) biogeochemistry is its near ubiquitous complexation by strong organic ligands; in the ocean >99% of dissolved Cu is organically complexed (e.g., Coale and Bruland, 1988; Moffett and Dupont, 2007; Bruland et al., 2013). The isotopic composition of Cu in seawater is more sparsely documented than that of Zn. Existing data also point to a homogeneous deep ocean, at about +0.66‰ (δ^{65}Cu relative to NIST SRM 976), with deviations towards lighter Cu isotope compositions (of about +0.30‰) in the surface ocean and along some continental margins, which appear to be associated with particulate Cu input (Takano et al., 2014; Thompson and Ellwood, 2014; Little et al., 2018; Baconnais et al., 2019).

Cold water corals grow at shallow to lower bathyal water depths (bathyal zone: 1000 – 4000 m), and occasionally in deeper waters (Roberts et al., 2009), and therefore offer potential as an archive of intermediate and deep ocean δ^{66}Zn and δ^{65}Cu values. While the upper water column cycling of Zn and Cu isotopes is complex and incompletely understood, the relative homogeneity of modern intermediate and deep ocean Zn (and presumably, albeit to a lesser extent, Cu) isotope compositions reflects the first-order role of water masses originating from the Southern Ocean in setting global oceanic nutrient distributions (Sarmiento et al., 2004; Vance et al., 2017; de Souza et al., 2018; Sieber et al., 2020). Today, the absence of significant biological Zn isotope

fractionation in the surface Southern Ocean (Zhao et al., 2014; Wang et al., 2018; Sieber et al., 2020) leads to the formation and advection northwards of intermediate (i.e. Sub-Antarctic Mode Water, SAMW, and Antarctic Intermediate Water, AAIW) and deep (Antarctic Bottom Water, AABW) water masses with the same (or very similar) isotopic compositions (Sieber et al., 2020). However, the physical, biogeochemical, and ecological characteristics of the Southern Ocean have changed through time (Sigman et al., 2010). For example, alleviation of Fe limitation in the past may have dramatically affected the nutrient status (and isotopic composition) of glacial analogues of AAIW and SAMW, as proposed for Si (e.g., Brzezinski et al., 2002; Matsumoto et al., 2002). Therefore, intermediate and deep-water Zn and Cu isotope compositions archived in cold-water corals could be used to trace past changes in biological utilization in the Southern Ocean, with implications for the global ocean carbon cycle.

In this study we evaluate the potential of cold-water corals as archives of seawater Zn and Cu isotopes. We present a series of physical and chemical cleaning experiments, followed by δ^{66}Zn, δ^{65}Cu, and trace element data for a suite of modern and late Holocene (<1500 yr old) cold-water corals from six oceanic regions spanning the North Atlantic to the Tasman Sea. Coral aragonite δ^{65}Cu values are distributed around the modern deep ocean Cu isotope composition, but exhibit significant scatter. The outlook for Zn is more promising, with reasonable agreement between coral aragonite δ^{66}Zn values and measured or best estimate modern seawater δ^{66}Zn values. A small number of older fossil specimens, dated to the last glacial period, were also analysed. These corals have Zn and Cu isotope compositions similar to modern seawater values, hinting at the relative constancy of oceanic Zn and Cu cycling on glacial-interglacial timescales.

2. Samples and Analytical Methods

2.1 Samples

The term cold-water coral (or alternatively deep-water coral) is used here to refer to azooxanthellate scleractinian corals, of which ~90 % live in deep or cold water (Roberts et al., 2009). Specimens in this study are solitary aragonitic corals of the species

Desmophyllum dianthus and genera *Caryophyllia* and *Dasmosmilia*. Taxonomic classification of samples was carried out in previous studies (listed below). *Caryophyllia* is the most diverse genus of cold-water corals, consisting of at least 66 species (Kitahara et al., 2010a). Genetic studies have highlighted the similarity of extant *Caryophyllia* and *Dasmosmilia* genera (Kitahara et al., 2010b).

Two *D. dianthus* specimens of glacial age, with well-developed black or brown surface coatings (due to the presence of Fe-Mn oxide phases), were selected for cleaning experiments (described in section 2.2). Twenty modern or late Holocene (<1500 yr old) coral specimens were then sampled, cleaned following the finalised cleaning procedure (section 2.2), and analysed for trace element concentrations and Zn and Cu isotopes (Table 1A). Finally, four corals dated to the last glacial period (including the two specimens used in cleaning experiments) were sampled and analysed for trace element concentrations and Zn and Cu isotopes (Table 1B).

Coral samples from water depths of 170 – 2260 m were selected from the following locations (Fig. 1; Table 1): south of Iceland (Reykjanes Ridge), the northwest Atlantic (Manning and Muir Seamount), the eastern equatorial Atlantic (Carter Seamount), the Drake Passage (Burdwood Bank and Sars Seamount), the southwest Indian Ocean (SWIO: Coral Seamount, Melville Bank, Atlantis Bank), and south of Tasmania (South Hills and St Helens seamounts). The corals selected from these collections have previously been described and dated by uranium-series or radiocarbon in: Burke (2012), Robinson et al. (2007), Chen et al. (2016), Margolin et al. (2014), Pratt et al. (2019), and Thiagarajan et al. (2013).

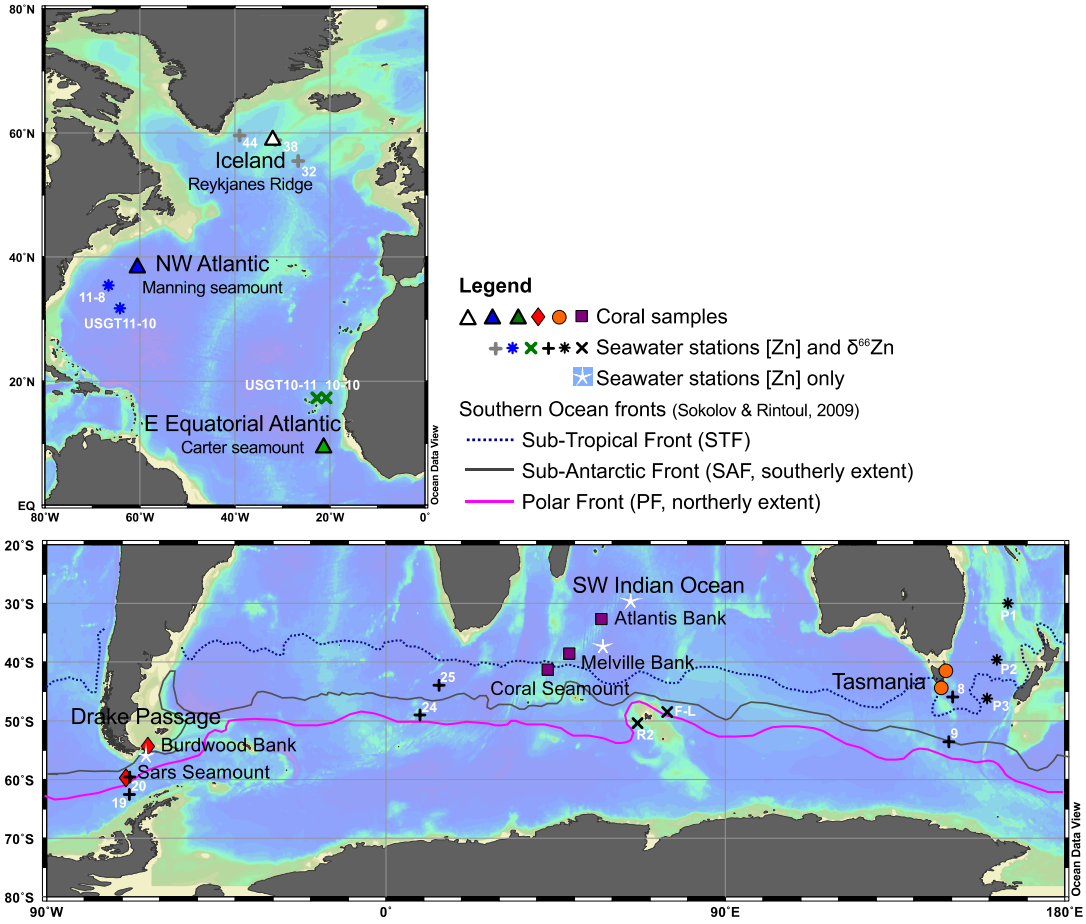

Figure 1. Maps showing the locations of Holocene coral specimens (filled symbols) and their nearest or most closely equivalent seawater sampling locations (❋ ✕ + ☆). Locations of the major Southern Ocean fronts are also shown (after Sokolov and Rintoul, 2009). Proximal seawater stations with published Zn isotope compositions as follows: Iceland, grey + (Lemaitre et al., 2020); North Atlantic, blue ❋ and green ✕ (Conway and John, 2014); Southern Ocean, black + (Sieber et al., 2020), black ✕ (Wang et al., 2018); Tasman Sea, black ❋ (Samanta et al., 2017). Seawater stations with Zn concentrations only (white ☆) from GEOTRACES IDP 2017 (Schlitzer et al., 2018). Station numbers are in white text.

2.2 Cleaning experiments

Fossil cold-water corals are often coated with a black-brown crust, made up of a mixture of iron and manganese oxides, incorporated detrital aluminosilicate grains, and occasional metal sulphides (Cheng et al., 2000). All these potential contaminating phases contain trace metals like Zn and Cu in concentrations that are orders of magnitude higher than those in coral aragonite (e.g., Boyle, 1981; Shen and Boyle,

1988). We tested the effectiveness of the physical and chemical cleaning procedures developed previously for cold-water corals (Shen and Boyle, 1988; Lomitschka and Mangini, 1999; Cheng et al., 2000; van de Flierdt et al., 2010; Crocket et al., 2014) for the analysis of Zn and Cu isotopes.

Two *D. dianthus* corals with a well-developed coating were selected for the cleaning experiments: DH115-DC-01 from the Drake Passage, and SS0108 from Tasmania (Table 1B). The black coatings of the two specimens were collected using a scalpel (coating samples were designated 'Coat'). Thereafter, 100 – 150 mg coral sub-samples were obtained using a Dremel tool and progressively subjected to increasingly rigorous cleaning steps (Figure 2):

- First, sub-samples of 'uncleaned' coral (designated 'UNCL') were rinsed three times in DI water, where rinsing refers to ultrasonication of the coral fragments in DI water in acid-cleaned 15 mL centrifuge tubes for 60 seconds, followed by removal of the supernatant by pipette.
- Second, three to four sub-samples were carefully physically cleaned using a Dremel tool and rinsed three times in DI water (designated 'PHYS'). During physical cleaning, any coatings were removed, as well as epibiont boreholes and other discoloration or impurities within the skeleton, including remineralised or secondary calcium carbonate.
- Third, three to four sub-samples were subject to physical cleaning and an oxidising chemical 'pre-cleaning' procedure (designated 'OXIC'). The chemical pre-cleaning procedure consisted of ultrasonication in a series of oxidative cleaning solutions, targeting residual organic phases (Shen and Boyle, 1988), with rinses in DI water (for details, see Figure 2).
- Finally, three to four sub-samples were subjected to the full physical and chemical cleaning procedure described by van de Flierdt et al. (2010) and detailed in Figure 2 (designated 'FULL'). The major difference between the pre-cleaning and full chemical cleaning procedures is the addition of a reductive cleaning step, which aims to remove trace metals associated with residual iron and manganese oxides (van de Flierdt et al., 2010).

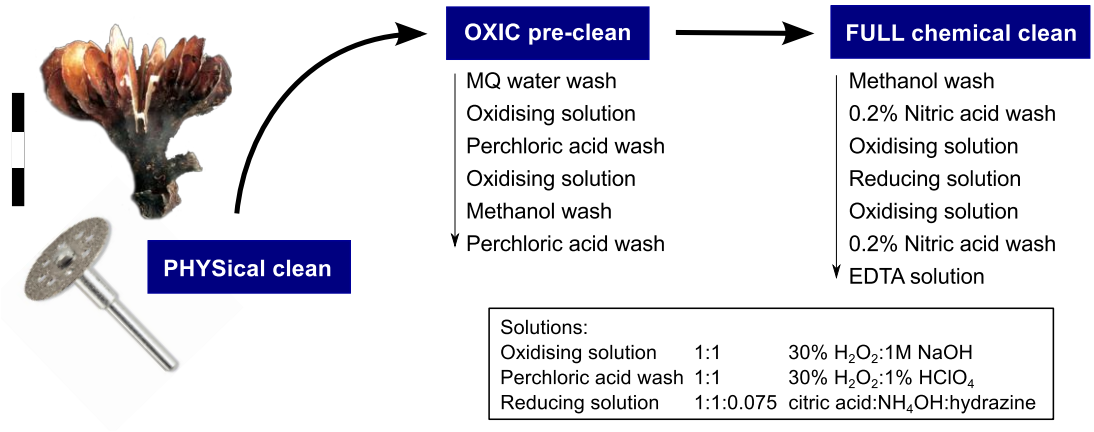

Figure 2. Schematic illustration of the protocol for progressive cleaning of coral samples, based on van de Flierdt et al. (2010).

For all other coral specimens for which data are reported in this study, sub-samples of 80-200 mg were subjected to the full physical and chemical cleaning procedure (Figure 2). Chemical cleaning led to an average mass loss of 7.0 ± 3.5% (1SD, n = 36, range 1.9 – 21%). Where possible, samples were analysed for Zn and Cu isotope compositions in duplicate (i.e. two coral sub-samples were separately cleaned, digested, and analysed). Four of the Holocene corals and all four glacial-age coral specimens had well-developed coatings (Table 1), which were also analysed to evaluate the possibility of residual contamination by Fe-Mn oxide or detrital (aluminosilicate) phases.

2.3 Analytical procedures

Sample digestion and column chemistry was carried out in the MAGIC clean laboratories at Imperial College London. Throughout, deionized 18.2 MΩ water (MQ), Teflon-distilled acids (HNO_3 and HCl), Suprapur H_2O_2, and acid-cleaned Savillex PFA labware were used. In preparation for analysis, corals and coatings were carefully bulk digested in 1 mL 6M HCl (carbonate effervesces vigorously on addition of acid). For coral samples with significant coatings, residual contamination was assessed using a mass balance approach and found to be negligible (see section 4.2, Table S3). Samples were then dried and redissolved in 5 mL 1M HCl.

An aliquot of this coral digest solution was diluted in 2% HNO_3 to give approximately 100 ppb Ca concentrations for multi-element analysis on a Thermo Element XR at ETH Zürich. The elements Li, Na, Mg, Al, Mn, Fe, Cu, Zn, Sr, Cd, Ba, and U were measured

as metal/Ca ratios following the procedure outlined in Hasenfratz et al. (2017). Accuracy and precision of the instrument were assessed by routine measurements of four consistency standards (Table S1), of which three are gravimetrically prepared in-house standards (CS1, CS2, CS3) and one is a carbonate rock standard purchased from LGC Standards (NCS DC70303).

The appropriate volume of a ^{64}Zn-^{67}Zn double spike was added to all samples to achieve a spike:sample ratio of approximately 1.2 (Arnold et al., 2010; Bridgestock et al., 2014). In order to obtain ≥ 40 ng Zn for isotope analysis, some sub-samples from the cleaning experiments were combined (Table 2). The Zn and Cu fractions were then purified using a two-step column chromatography procedure using AG MP-1M resin (BioRad), as detailed previously (Maréchal et al., 1999; Archer and Vance, 2004; Little et al., 2014). The second Zn column was smaller in volume, following Bridgestock et al. (2014). Prior to analysis, purified Zn and Cu fractions were oxidised by treatment with 2 × ~100 µL 14 M HNO_3 (Zn) or refluxing overnight with 14 M HNO_3 + H_2O_2 (Cu), before final dissolution in 2% HNO_3. Procedural Zn and Cu blanks were < 1 ng.

Cleaned coral Zn concentrations and Zn/Ca ratios were calculated using isotope dilution (Zn/Ca_{ID}, based on data from the Nu Plasma) for comparison with Element-derived ($Zn/Ca_{Element}$) ratios. Calcium concentrations (required to calculate Zn/Ca ratios) were estimated based on the mass of the coral sub-sample and molecular mass of $CaCO_3$. $Zn/Ca_{Element}$ and Zn/Ca_{ID} are typically in agreement, with $Zn/Ca_{Element}$ = 113 ± 29% of Zn/Ca_{ID} (1SD, n = 33). However, Element-derived Zn/Ca ratios approach blank levels (i.e. detection limit) at the very low Zn concentrations found in cleaned corals, hence Zn and Zn/Ca values from isotope dilution are reported in Tables 2-4.

Analytical protocols for isotopic analysis have been described previously for Cu in Little et al. (2014, 2017) and for Zn in Arnold et al. (2010), Bridgestock et al. (2014), and Little et al. (2019). Both Cu and Zn isotope ratios were blank-corrected using a prior analysis of the 2% HNO_3 solution used to dilute the samples. In brief, Cu isotope ratios were analysed in low resolution mode on a Neptune Plus MC-ICP-MS at ETH Zürich. Sample introduction was via a Savillex C-Flow PFA nebuliser (50 µl/min) attached to a glass spray chamber. Copper isotope ratios for samples were calculated

using a standard bracketing approach by comparison to pure untreated NIST SRM 976 and are reported relative to this standard in delta (per mil, ‰) notation:

$$\delta^{65/63}\mathrm{Cu} = \left(\frac{(^{65}\mathrm{Cu}/^{63}\mathrm{Cu})_{\mathrm{sample}}}{(^{65}\mathrm{Cu}/^{63}\mathrm{Cu})_{\mathrm{SRM\ 976}}} - 1\right) \times 1000 \quad (1)$$

Samples analysed for Cu isotope compositions on two measurement days, including the initial analysis of cleaning experiments from DH115-DC-01, the first batch of Holocene samples, and one SS0108 sub-sample (FULL-4), exhibited anomalously light Cu isotope signatures and apparently elevated Cu concentrations (as calculated from beam-matching during the isotopic analysis) compared to those measured prior to chemistry using the Element ICP-MS. These samples did not show elevated Na or Mg concentrations after chemistry, but the presence of an unidentified isobaric interference on ^{63}Cu, or contamination, is considered probable. These data are excluded from the final datasets presented in Tables 2 and 4. Copper samples from all subsequent batches of Holocene and glacial-age corals, and duplicated cleaning experiment samples for DH115-DC-01, were subject to a third Cu clean-up column and no further discernible issues were encountered.

Zinc isotope ratios were analysed in low resolution mode at Imperial College London on a Nu Plasma HR MC-ICP-MS equipped with an ARIDUS II (CETAC Technologies) desolvating system and nominal 100 µL/min MicroMist glass nebulizer. Instrumental mass bias was corrected via a double-spike technique (Arnold et al., 2010) using the offline data-reduction procedure of Siebert et al. (2003). Interference corrections for ^{64}Ni (monitoring mass 62) and Ba^{2+} (monitoring mass 68.5) were negligible. The Zn isotope ratios of samples were determined relative to matching (spike:natural Zn ratio and total Zn) standard solutions of IRMM-3702:

$$\delta^{66/64}\mathrm{Zn} = \left(\frac{(^{66}\mathrm{Zn}/^{64}\mathrm{Zn})_{\mathrm{sample}}}{(^{66}\mathrm{Zn}/^{64}\mathrm{Zn})_{\mathrm{IRMM\text{-}3702}}} - 1\right) \times 1000 \quad (2)$$

Final δ^{66}Zn values are reported normalised to JMC Lyon by applying a correction of +0.30‰, as recommended by Moynier et al. (2017).

Accuracy and reproducibility of $\delta^{66}Zn$ and $\delta^{65}Cu$ values were assessed by repeated analysis of secondary solution standards (London Zn, AM Cu), as well as digestion and analysis of several USGS rock standards (Nod P1, BCR-2, BHVO-2, BIR-1, SGR-1), and a carbonate consistency standard (NCS DC70303), and are reported in Table S2. Data for these standards agree with literature values, where available (Bigalke et al., 2010; Moynier et al., 2017). Error bars on figures are the external 2SD reproducibility of the carbonate consistency standard (NCS DC70303: $\delta^{65}Cu = 0.21 \pm 0.11‰$, $\delta^{66}Zn = 0.76 \pm 0.07‰$) or internal 2SE on individual isotope ratios, whichever is larger.

3. Results

3.1 Cleaning experiments

Illustrative results from the cleaning experiments are presented in Figure 3 (Tasmanian coral SS0108) and Figure 4 (Drake Passage coral DH115-DC-01), with the complete dataset given in Table 2 and further metal/Ca ratio cross-plots in Figure S1 and Figure S2. Trace element/calcium ratios decrease with progressive cleaning, with Zn/Ca and Cu/Ca ratios in fully cleaned samples a factor of 5-10 lower than in uncleaned samples, and two to three orders of magnitude lower than in the coral coatings (Figs. 3, 4, S1, S2; Table 2). Copper is most closely correlated with Mn concentrations, and Zn with Fe concentrations, but strong correlations exist between all four elements, and with Al (Figs. 3, 4, S1, S2). As a result, distinguishing the contributions of Fe oxides, Mn oxides, and detrital contaminants on the basis of metal/Ca ratios is precluded.

Coating $\delta^{65}Cu$ values (–0.01‰, +0.23‰) are more negative than cleaned coral aragonite, consistent with Cu derived from a mixed lithogenic (i.e. detrital silicates, at about 0‰; Moynier et al., 2017) and/or authigenic Fe-Mn oxide source (at about +0.3‰; Albarède, 2004; Little et al., 2014, 2017). Coating $\delta^{66}Zn$ values (+0.55‰, +0.25‰) can be either more positive or negative than coral aragonite, reflecting the diverse Zn isotope compositions in potential contaminating material. The Zn isotope composition of lithogenic (i.e. detrital silicates) and authigenic Fe-Mn oxide sources are expected to be about +0.3‰ (Moynier et al., 2017) and +1‰ (Maréchal et al., 2000; Little et al., 2014), respectively.

Fully cleaned coral Cu concentrations for the two cleaning specimens are 0.2 to 0.4 µg/g, with Cu/Ca ratios of 0.4 to 0.7 µmol/mol and δ^{65}Cu values ranging from +0.69 to +0.89‰. Fully cleaned Zn concentrations are 0.37 to 0.67 µg/g, with Zn/Ca ratios of 0.38 to 0.68 µmol/mol and δ^{66}Zn values of +0.34 to +0.40‰. For these two coral specimens, thorough physical cleaning appears to be effective in removing Zn associated with the coating, leading to similar results to those of fully chemically cleaned samples (Figs. 3 and 4, C and D). Interestingly, Wilson et al. (2017) also found that physical cleaning is more important than chemical cleaning for removing anthropogenic Pb from fossil corals. In contrast, the full cleaning procedure has a marked impact on Cu/Ca and δ^{65}Cu of the Tasmanian coral compared to the physically cleaned and oxidatively cleaned aliquots (Fig. 3A and B).

Finally, the fully cleaned Zn and Cu isotope compositions of both corals subject to cleaning experiments are comparable to modern day seawater Zn (δ^{66}Zn = +0.45 ± 0.14‰, 2SD, data >200m in Southern Ocean or >600m elsewhere; Conway and John, 2014, 2015; Zhao et al., 2014; Samanta et al., 2017; John et al., 2018; Vance et al., 2019; Lemaitre et al., 2020; Liao et al., 2020; Sieber et al., 2020) and Cu (δ^{65}Cu = +0.66 ± 0.19‰, 2SD, data >200m; Takano et al., 2014; Thompson and Ellwood, 2014; Little et al., 2018) isotope compositions (Figs. 3 and 4). We also note that Zn/Ca ratios in cleaned samples vary by a factor of two for the Drake Passage coral, with no associated variability in δ^{66}Zn (Fig. 4C and D).

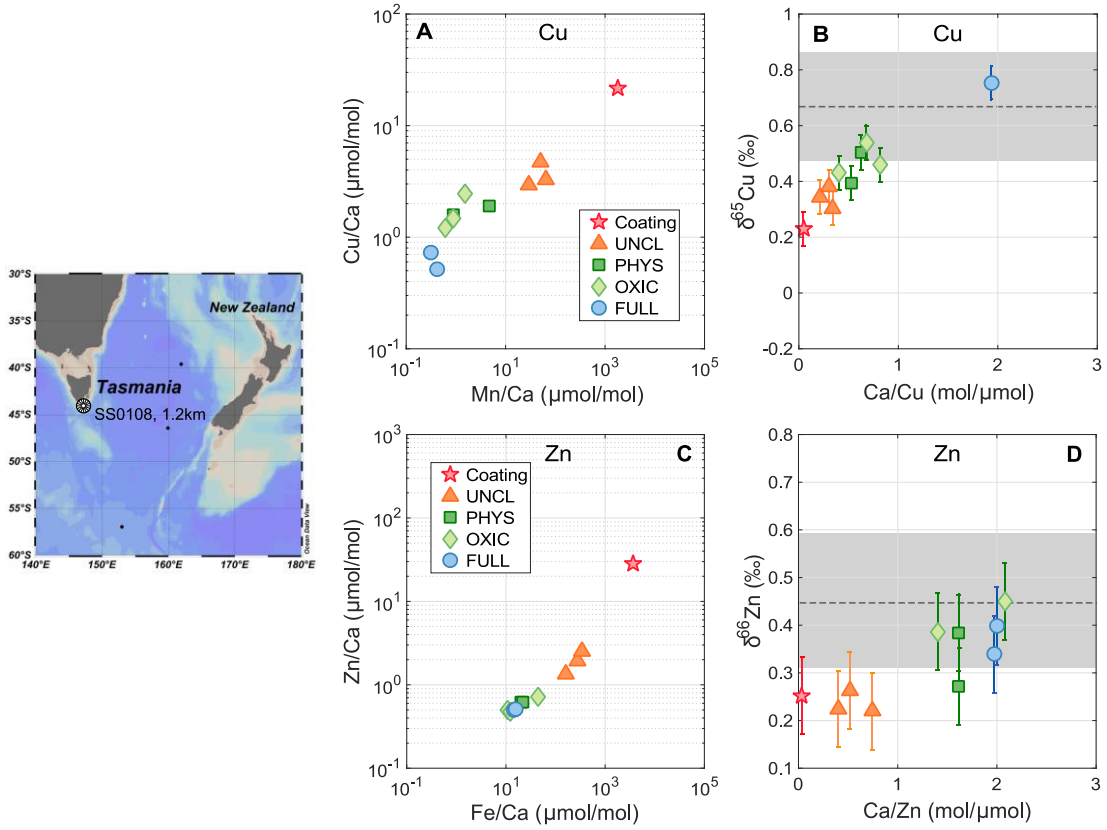

343

344 **Figure 3**. Illustrative results of the cleaning experiment on Tasmanian coral sample
345 SS0108. Inset map shows location of the coral and its water depth. Panels A and C
346 show Cu/Ca and Zn/Ca ratios of the cleaning aliquots versus trace element indicators
347 of contamination (Mn/Ca and Fe/Ca respectively); note log-log scales. Panels B and D
348 show δ^{65}Cu and δ^{66}Zn values versus the inverse of their concentration, as Ca/Cu and
349 Ca/Zn respectively. Dashed lines and grey bars represent the average and 2SD range of
350 modern deep seawater (δ^{66}Zn = +0.45 ± 0.14‰; δ^{65}Cu = +0.66 ± 0.19‰; see text for
351 references). Red stars represent the coral coating, orange triangles: uncleaned coral
352 aliquots, dark green squares: physically cleaned aliquots, light green diamonds:
353 physically and oxidatively pre-cleaned aliquots, and blue circles: fully cleaned samples.
354

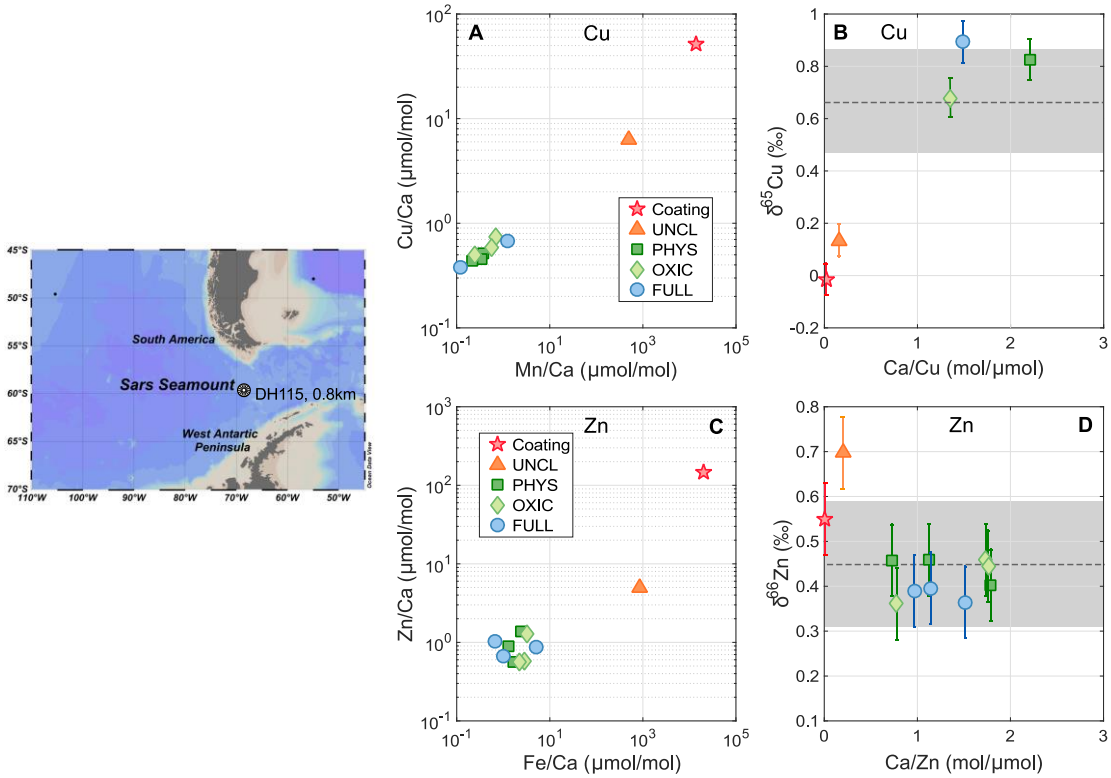

Figure 4. Illustrative results of the cleaning experiment on Drake Passage coral sample DH115-DC-01. Inset map shows location of the coral, from Sars Seamount, and its water depth. Panels A and C show Cu/Ca and Zn/Ca ratios of the cleaning aliquots versus trace element indicators of contamination (Mn/Ca and Fe/Ca respectively); note log-log scales. Panels B and D show $\delta^{65}Cu$ and $\delta^{66}Zn$ values versus the inverse of their concentration, as Ca/Cu and Ca/Zn respectively. Dashed lines and grey bars represent the average and 2SD range of modern deep seawater ($\delta^{66}Zn$ = +0.45 ± 0.14‰; $\delta^{65}Cu$ = +0.66 ± 0.19‰; see text for references). Symbols are as in Figure 3.

3.2 Holocene corals

3.2.1 Trace element/Ca ratios

For the fully cleaned Holocene coral samples, indicators of detrital or Fe-Mn oxide contamination (Fe/Ca, Mn/Ca, Al/Ca) are very low (Fig. S3; Table 3), with the exception of coral #17 from the northwest Atlantic (particularly sub-sample B). This sample remained visibly unclean after physical cleaning and has somewhat elevated Fe/Ca (6.7 and 15.2 µmol/mol for sub-samples A and B) and Al/Ca ratios (14.7 µmol/mol and 28.5 µmol/mol). Other samples typically exhibit Fe/Ca ratios < 2 µmol/mol (max: 3.8 µmol/mol), Mn/Ca ratios < 0.25 µmol/mol (max: 0.48 µmol/mol), and Al/Ca ratios that are below detection (max: 3.1 µmol/mol). By contrast, coral

coatings exhibit Mn/Ca, Fe/Ca, and Al/Ca ratios that are very variable (due to the variable carbonate content of the scrapings), but in all cases several orders of magnitude higher than those of the cleaned corals (Table 3). For comparison, Marchitto and Broecker (2006) compiled values for chemically cleaned benthic foraminifera of 4 – 51 (Fe/Ca) and 11 – 68 (Mn/Ca) µmol/mol, and Marchitto et al. (2005) limited palaeoceanographic interpretation of benthic foraminiferal Zn/Ca data to samples with Mn/Ca values of < 200 µmol/mol. Hence, the Fe/Ca and Mn/Ca ratios of our corals are typically at least an order of magnitude lower (up to three orders of magnitude lower for Mn/Ca) than those in foraminifera-based studies.

Cleaned samples of *D. dianthus* exhibit Zn/Ca ratios in a fairly tight range of 0.4 to 3.0 µmol/mol, while samples of *Caryophyllia* and *Dasmosmilia* spp. have much more variable and sporadically high Zn/Ca (range 0.3 – 17 µmol/mol; Table 3, Figs. 5, S3). No discernible species-related variability in Cu/Ca ratios is observed, with all samples in the range of 0.13 to 1.0 µmol/mol (Table 3, Figs. 5, S3). No relationships between Zn/Ca or Cu/Ca and Fe/Ca, Mn/Ca, or Al/Ca are present in the Holocene coral dataset (Fig. S3; Table 3). For the two sub-samples of coral #17, which exhibit elevated Fe/Ca and Al/Ca, Zn/Ca and Cu/Ca ratios are some of the lowest of the whole dataset (Zn/Ca: 0.52, 0.58 µmol/mol; Cu/Ca: 0.16, 0.22 µmol/mol).

3.2.2 Holocene coral $\delta^{66}Zn$ and $\delta^{65}Cu$ values

All fully cleaned coral duplicates are within analytical uncertainty for $\delta^{66}Zn$ and $\delta^{65}Cu$, based on the external 2SD reproducibility obtained for multiple analyses of a carbonate standard (± 0.07‰ and ± 0.11‰ respectively; Table 4). However, the results from duplicate analyses of sample #1 (Reykjanes Ridge) are at the limit of this definition of the uncertainty, both for $\delta^{66}Zn$ (+0.67‰, +0.55‰) and $\delta^{65}Cu$ (+0.45‰, +0.25‰). The two sub-samples of coral #17, with variably elevated Fe/Ca and Al/Ca (Table 3), are analytically indistinguishable in both $\delta^{66}Zn$ (+0.61‰, +0.54‰) and $\delta^{65}Cu$ (+0.62‰, +0.54‰).

Coral coatings exhibit $\delta^{66}Zn$ values of +0.25 to +0.90‰ and $\delta^{65}Cu$ values of –0.01 to +0.26‰ (Table 4), consistent with mixtures of detrital and authigenic Zn and Cu (as seen in the cleaning experiments). Coatings are also distinctly different in isotopic composition compared to their respective corals: both higher and lower $\delta^{66}Zn$ values

411 are observed in coatings compared to corals, while δ^{65}Cu values are always lower in
412 coatings (Table 4).
413
414 Figure 5 presents cleaned coral Zn and Cu isotope compositions compared to Ca/Zn
415 and Ca/Cu ratios respectively, with data differentiated by species or genera. The spread
416 in Holocene coral δ^{66}Zn values is from +0.07 to +0.67‰, with δ^{65}Cu values of +0.27
417 to +1.05‰. No systematic species-specific isotopic variability is evident in these small
418 datasets (Fig. 5). Most samples overlap the range of modern deep ocean isotopic
419 compositions (shaded blue bars) for Zn (+0.45 ± 0.14‰, 2SD, data >200m in Southern
420 Ocean or >600m elsewhere; Conway and John, 2014, 2015; Zhao et al., 2014; Samanta
421 et al., 2017; John et al., 2018; Vance et al., 2019; Lemaitre et al., 2020; Liao et al.,
422 2020; Sieber et al., 2020) and Cu (+0.66 ± 0.19‰, 2SD, data >200m; Takano et al.,
423 2014; Thompson and Ellwood, 2014; Little et al., 2018). There is some indication of a
424 weak trend in Ca/Zn versus δ^{66}Zn, with isotopically heavier Zn broadly linked to
425 samples with lower Zn concentrations (i.e. higher Ca/Zn ratios).

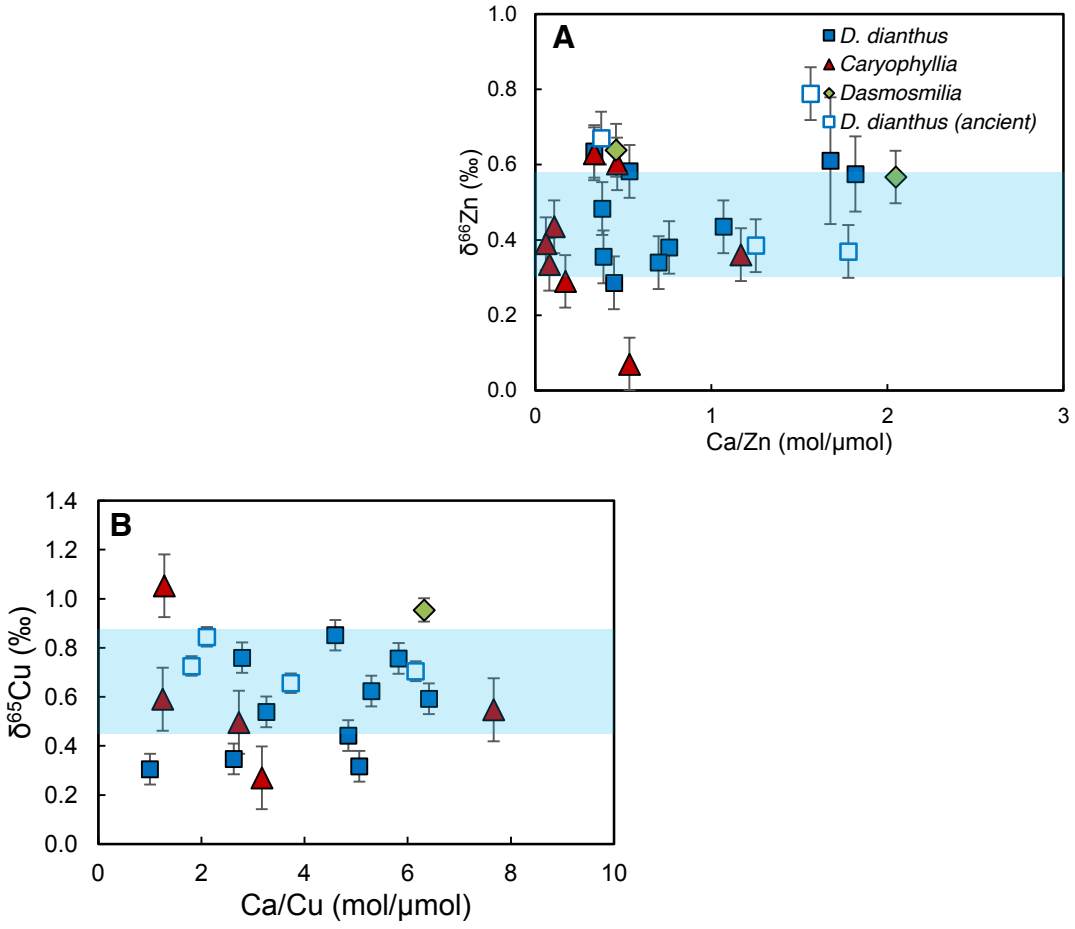

426
427
428 **Figure 5.** Coral (A) Zn and (B) Cu isotope compositions versus Ca/Zn and Ca/Cu ratios
429 respectively (mol/µmol), illustrated by species. Filled blue squares: Holocene *D.*

dianthus; filled red triangles: *Caryophyllia*; filled green diamonds: *Dasmosmilia*; unfilled blue squares: *D. dianthus* from the last glacial period. Blue bars represent the 2SD range of modern deep seawater ($\delta^{66}Zn = +0.45 \pm 0.14‰$; $\delta^{65}Cu = +0.66 \pm 0.19‰$; see text for references). Average Zn/Ca and Cu/Ca ratios are plotted for duplicate samples. Error bars are the external 2SD reproducibility of a secondary carbonate standard ($\delta^{66}Zn \pm 0.07‰$, $\delta^{65}Cu \pm 0.11‰$), or the internal 2SE of the isotopic analysis, whichever is larger.

3.3 Glacial corals

Indicators of detrital or authigenic Fe-Mn oxide contamination for the four *D. dianthus* specimens from the last glacial period are slightly elevated compared to the Holocene dataset, but remain low overall (Table 3). Glacial coral Al/Ca ratios range from below detection to 16.1 μmol/mol, Fe/Ca ratios from 2.0 to 13.3 μmol/mol, and Mn/Ca ratios from 0.1 to 1.2 μmol/mol. The ranges of glacial coral Zn/Ca (0.6 to 3.0 μmol/mol) and Cu/Ca (0.2 to 0.5 μmol/mol) ratios are very similar to their Holocene counterparts (Table 3; Fig. 5).

Isotopically, corals from the last glacial period overlap with the respective Holocene datasets, with the exception of a single sample from the equatorial Atlantic (sample #20) that expands the measured $\delta^{66}Zn$ range to +0.79‰ (Fig. 5; Table 4). The two North Atlantic corals have more positive $\delta^{66}Zn$ values (+0.79‰, +0.67‰) than the corals from the Southern Ocean and Tasman Sea (+0.37‰, +0.38‰). The range in $\delta^{65}Cu$ values for the four glacial specimens is from +0.66‰ to 0.84‰, with no systematic geographical variability (Table 4).

4. Discussion

4.1 Zn and Cu partitioning in cold-water coral aragonite

Best estimates for ambient seawater Zn and Cu concentrations were compiled by extrapolating along isopycnals from the nearest seawater profile or, in the southwest Indian Ocean where data is sparse, the most oceanographically equivalent profile based on proximity to Southern Ocean fronts (Fig. 1, Table 4). Assuming that Ca is uniformly

distributed in the ocean at a concentration of 10.3 mmol kg^{-1}, we calculate apparent partition coefficients for each coral specimen as follows (Table 4):

(3) $D_{Zn} = [Zn/Ca]_{coral} / [Zn/Ca]_{seawater}$

(4) $D_{Cu} = [Cu/Ca]_{coral} / [Cu/Ca]_{seawater}$

Note that reported Zn concentrations in and around the active hydrothermal vent site of the Reykjanes Ridge range widely from 1.4 to 6 nmol/kg (Lemaitre et al., 2020), while Cu concentrations at this location are poorly defined. Previous work has also found that Ba partitioning in these Icelandic corals is unusual compared to corals from elsewhere in the Atlantic and Southern Ocean, indicating a possible site-specific effect in this location (Hemsing et al., 2018; Spooner et al., 2018). Therefore, the two Icelandic corals are excluded from the description of elemental partitioning that follows.

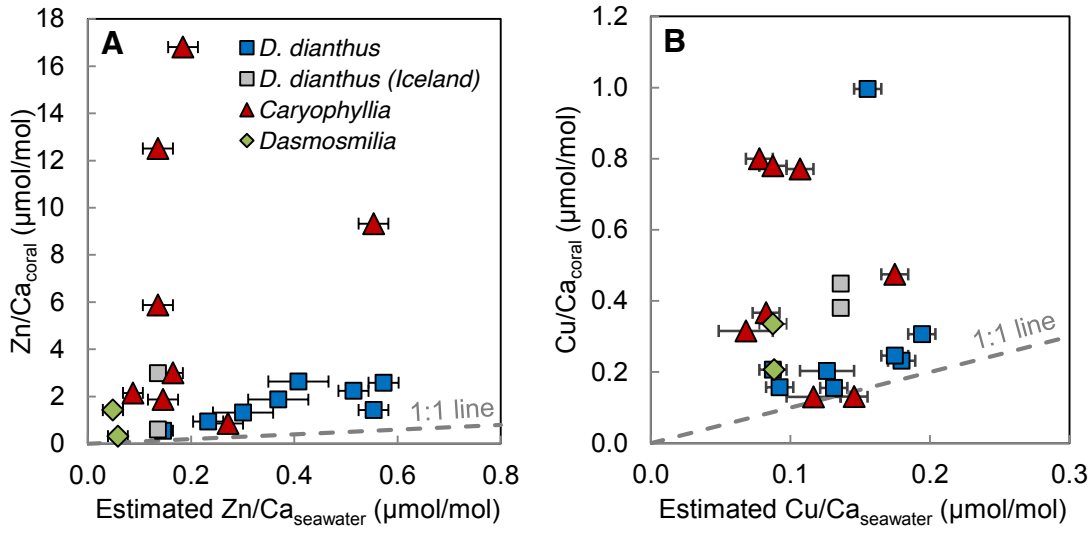

Figure 6. (A) Comparison of Holocene coral Zn/Ca ratios with estimated ambient seawater Zn/Ca ratios (for references, see Table 4) and (B) coral Cu/Ca ratios with estimated seawater Cu/Ca ratios, by coral species. Average Zn/Ca_{coral} and Cu/Ca_{coral} ratios are plotted for duplicate samples. Blue squares: *D. dianthus*; red triangles: *Caryophyllia*; green diamonds: *Dasmosmilia*. Grey squares are *D. dianthus* specimens from Iceland, for which ambient seawater Zn and Cu concentrations (and thus Zn/Ca and Cu/Ca) are poorly constrained; for example, reported Zn concentrations at stations close to the Reykjanes Ridge range from 1.4 to 6 nmol/kg (Lemaitre et al., 2020). Grey dashed lines represent partition coefficients of 1 (e.g., $Zn/Ca_{coral} = Zn/Ca_{seawater}$).

Zinc and Cu partitioning in *D. dianthus* specimens is generally uniform, with $D_{Zn} = 4.4 \pm 2.2$ (2SD; excluding Icelandic corals), and $D_{Cu} = 1.4 \pm 1.0$ (2SD; excluding Icelandic corals and sample #21 with $D_{Cu} = 6.4$). Calculated D_{Zn} values for *Caryophyllia* and *Dasmosmilia* are generally elevated and more variable than those of *D. dianthus*,

492 ranging between 3.1 and 92 (Table 4). Similarly, calculated D_{Cu} values for *Caryophyllia*
493 and *Dasmosmilia* are also more variable than for *D. dianthus*, at 0.9 to 10.
494
495 We also observe significant intra-coralline variability in Zn/Ca and Cu/Ca ratios for
496 specimens that were separately sub-sampled and analysed more than once. For
497 example, for the glacial-age Drake Passage coral DH115-DC-01, which was subject to
498 the cleaning experiment and thus analysed on multiple occasions, the range in Zn/Ca
499 ratios for all 'cleaned' samples (i.e. all physically and chemically cleaned samples, n =
500 12) is 0.37 – 0.90 μmol/mol. For the 'fully cleaned' samples only (n = 4), the Zn/Ca
501 range is similar, at 0.38 – 0.68 μmol/mol. For Cu, the equivalent intra-specimen
502 variability is 0.37 – 0.80 μmol/mol for all 'cleaned' samples, or 0.37 – 0.67 μmol/mol
503 for 'fully cleaned' samples. Taken at face value, such differences would imply intra-
504 coralline variability in D_{Zn} and D_{Cu} for *D. dianthus* of approximately a factor of two,
505 similar to the variability in partitioning between individual specimens (Fig. 6).
506
507 Intra-coralline variability could be structural, since differences in trace element/Ca
508 ratios have been observed between centres of calcification (COC) and regions of fibrous
509 aragonite. For example, Mg/Ca and Li/Ca ratios are significantly enriched in COCs
510 (Gagnon et al., 2007; Meibom et al., 2008; Case et al., 2010; Anagnostou et al., 2011).
511 This variability has been proposed to reflect either Rayleigh fractionation processes
512 (e.g., Gagnon et al., 2007; Case et al., 2010) or differences in precipitation rate, with
513 COCs precipitating more rapidly than fibrous regions (Gabitov et al., 2008; Brahmi et
514 al., 2012). It has also been suggested that Mg may be more easily incorporated into
515 organic compounds or amorphous calcium carbonate than substituted for Ca in the
516 aragonite lattice, with the former components both thought to be more prevalent in
517 COCs than surrounding fibres (Cuif et al., 2003; Finch and Allison, 2008; Rollion-Bard
518 et al., 2010). Since sub-samples of individual coral specimens can be expected to
519 include carbonate from COCs and fibrous regions in differing proportions, the observed
520 intra-specimen variability in Zn and Cu concentrations hints at similar controls on the
521 partitioning of these elements. Hence, future work should employ high sensitivity,
522 microanalytical techniques to evaluate the distribution of Zn and Cu in COCs versus
523 fibrous aragonitic regions of cold-water corals.
524
525

4.2 Comparison of cold-water coral and seawater Zn and Cu isotope compositions

Most Holocene cold-water coral $\delta^{66}Zn$ values are within uncertainty of ambient seawater $\delta^{66}Zn$ values (Figs. 5, 7). For each specimen, the parameter $\Delta^{66}Zn_{coral\text{-}sw}$ is calculated, where:

$$\Delta^{66}Zn_{coral\text{-}sw} = \delta^{66}Zn_{coral} - \delta^{66}Zn_{seawater} \quad (5)$$

For the complete Holocene dataset, we find $\Delta^{66}Zn_{coral\text{-}sw} = +0.03 \pm 0.17‰$ (1SD, n = 20) (Fig. 8; Table 4). Therefore, the first order finding of this study is that coral aragonite appears to incorporate Zn from seawater without isotopic fractionation. In addition, live-collected and fossil Holocene corals from similar depths overlap in $\Delta^{66}Zn_{coral\text{-}sw}$, with no perceptible diagenetic modification of coral Zn isotope compositions (Fig. 8). Furthermore, at the resolution of this study (i.e. bulk analysis of ca. 100mg coral aliquots), intra-coralline variability in Zn/Ca (section 4.1) is not associated with resolvable variability in $\delta^{66}Zn$ (Figs. 3, 4).

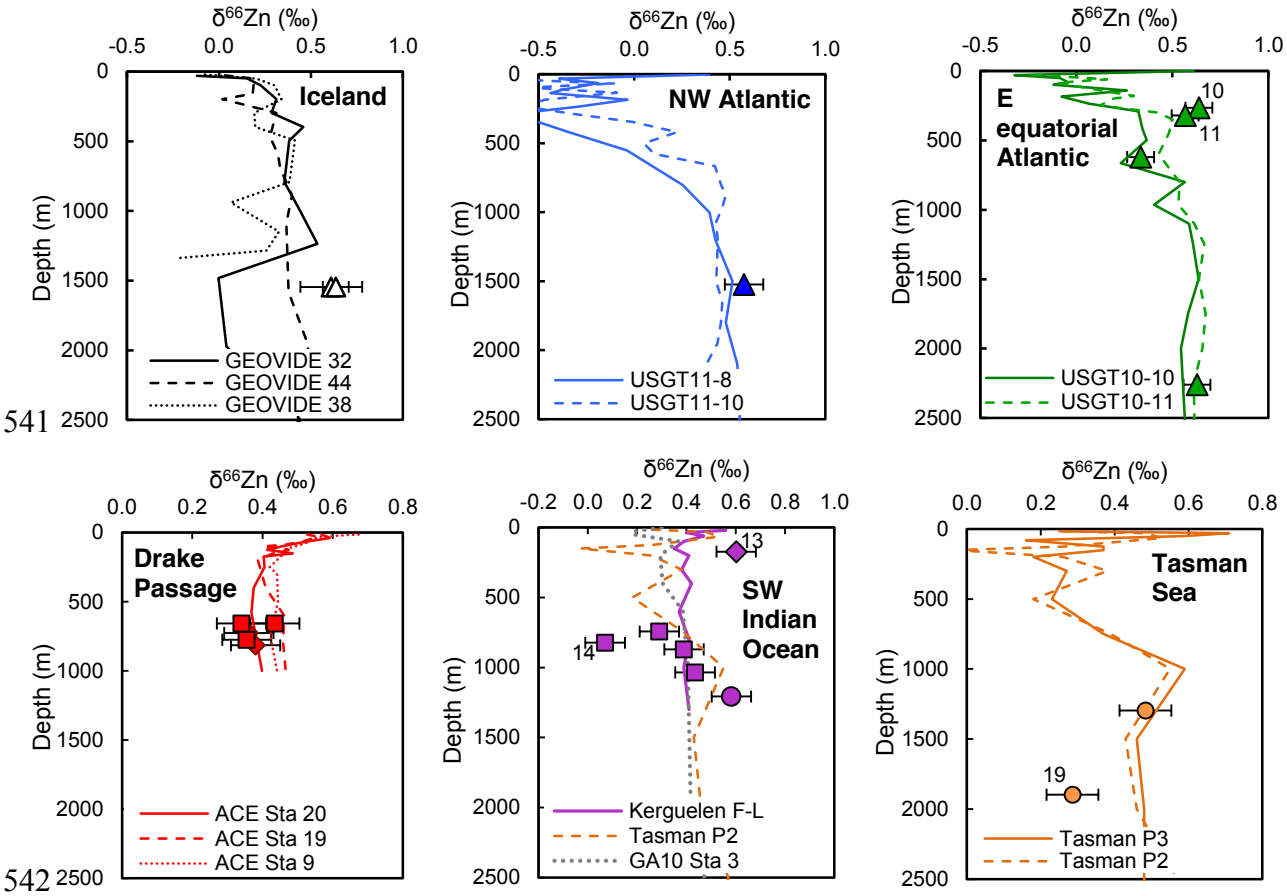

Figure 7. Zinc isotope composition of Holocene corals versus water depth, plotted by geographic location. Atlantic corals are shown by triangles. Open triangles: Reykjanes Ridge, Iceland; blue triangle: Manning Seamount, NW Atlantic; green triangles: Carter

Seamount, eastern equatorial Atlantic. Drake Passage corals are red squares (Sars Seamount) and red diamonds (Burdwood Bank). SW Indian Ocean corals are purple squares (Atlantis Bank), diamond (Melville Bank) or circle (Coral Seamount). Tasmanian corals are orange circles. Local or most oceanographically equivalent seawater profiles (determined by water mass comparisons and neutral density estimates) are shown in solid, dashed, or dotted lines (individual panel legends, see Fig. 1 and Table 4 for locations and references). Corals discussed in the text (i.e. those notably offset from ambient seawater) are labelled with their respective sample numbers (see also Fig. 8).

However, the dataset exhibits some scatter in $\Delta^{66}Zn_{coral\text{-}sw}$, with several specimens that exhibit higher or lower $\delta^{66}Zn$ values compared to ambient seawater (Figs. 7, 8). The simplest explanation for scatter in $\Delta^{66}Zn_{coral\text{-}sw}$ would be the presence of Zn from residual contaminating phases, i.e. Fe-Mn oxides or detrital grains. For those corals with a well-developed coating, the contribution from any residual coating to the Zn budget of a cleaned coral can be estimated as follows:

$$[Zn]_{coating\ contribution} = [Fe]_{coral} \times \left(\frac{Zn}{Fe}\right)_{coating} \quad (6)$$

In this equation, Zn can be replaced by Cu, and Fe can be replaced by another indicator of contamination, such as Mn. Coating Zn contributions of 0.0 – 3.0% based on Fe (or 0.0 – 3.6% based on Mn) are calculated for seven of eight corals (Table S3). For a single glacial-age sample (SS0108), this approach yields an estimate of 21% based on Fe (or 1.2% based on Mn) (Table S3). For Cu, the equivalent coating contributions are 0.4 – 14% based on Fe (or 0.0 – 17% based on Mn). Mass balance can then be applied to correct the measured isotopic compositions of cleaned corals using paired coral and coating $\delta^{66}Zn$ and $\delta^{65}Cu$ values (Table S3). In all cases, the corrected and uncorrected isotopic compositions overlap within measurement uncertainty, with a maximum correction of +0.03‰ for Zn and +0.08‰ for Cu (in both cases for the glacial coral SS0108, based on Fe). It therefore appears unlikely that the observed scatter in $\Delta^{66}Zn_{coral\text{-}sw}$ (Fig. 8) can be the result of residual contaminating phases.

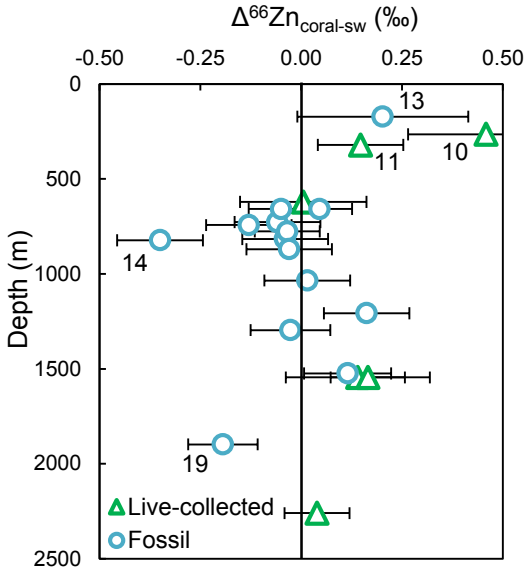

Figure 8. The offset between Holocene coral and ambient seawater $\delta^{66}Zn$ values, reported as $\Delta^{66}Zn_{coral\text{-}sw}$, versus water depth. Live-collected corals are shown as green triangles, with fossil corals shown as blue circles. Error bars are the propagated uncertainty from coral and seawater compositions. Corals discussed in the text (i.e. those notably offset from seawater values) are labelled with their respective sample numbers (see also Fig. 7).

One observation that may indicate a systematic rather than random occurrence of samples with a $\Delta^{66}Zn_{coral\text{-}sw}$ offset is that the three corals from the upper 0.5 km of the water column (samples #10 and #11 from the eastern equatorial Atlantic, #13 from the SW Indian Ocean; Table 4) have positive $\Delta^{66}Zn_{coral\text{-}sw}$ values (i.e. they are isotopically heavier than seawater; Fig. 8). A possible explanation for these offsets is that the estimates of ambient seawater $\delta^{66}Zn$ values are inaccurate; to explain positive coral $\Delta^{66}Zn_{coral\text{-}sw}$ values, the seawater values must be too low. This scenario is most likely to arise for the upper water column, where seawater $\delta^{66}Zn$ values are highly variable and, outside of the Southern Ocean, excursions towards low sub-surface $\delta^{66}Zn$ values are frequently observed (e.g., see Fig. 7; Conway and John, 2014; Samanta et al., 2017; Vance et al., 2019; Lemaitre et al., 2020; Liao et al., 2020). The origin of these isotopically light excursions is a subject of active debate, but a link to anthropogenic aerosol input has been proposed (Lemaitre et al., 2020; Liao et al., 2020), which would imply that they are a recent phenomenon. Estimated cold-water coral growth rates are on the order of 0.5-2 mm/yr (Adkins et al., 2004), hence a single isotope analysis is likely to represent a few decades to a century of coral growth. Therefore, even though two of the three upper water column corals in this study were collected alive, it is

plausible that all three corals lived a substantial portion of their lives in seawater with a Zn isotope composition that was heavier than observed in the modern-day.

Two fossil samples from deeper water have negative $\Delta^{66}Zn_{coral\text{-}sw}$ values (#14 at 0.8 km depth from Atlantis Bank in the SW Indian Ocean, #19 at 1.9 km depth from South Hills, Tasmania; Fig. 8, Table 4). Deep seawater $\delta^{66}Zn$ values are generally homogeneous, so these results are difficult to explain. The isotopic composition of sample #19 from Tasmania is +0.29‰, comparable to the lithogenic Zn isotope composition (at about +0.3‰), but the trace element data provides no indication of detrital contamination (e.g., Al/Ca ratio is below detection; Table 3). Sample #14, from Atlantis Bank, is even lighter, at +0.07‰, and seems to be anomalous as three other corals (#16, #22, #23) from similar depths (743 – 1035m) at Atlantis Bank have values of +0.44‰, +0.29‰ and +0.39‰. These anomalies could potentially derive from the chemical cleaning procedure: several studies have suggested that the inclusion of a reductive cleaning step can lead to analytical artefacts (Pichat et al., 2003; Yu et al., 2007; Clarkson et al., 2020), including anomalous shifts to more negative $\delta^{66}Zn$ values in carbonates (Druce, 2021).

To fully resolve the origin of the observed positive (and occasional negative) $\Delta^{66}Zn_{coral\text{-}sw}$ values, and the extent to which they represent a potential source of new information versus a limitation of the proxy archive, will require a larger dataset of cold-water coral data and better observational constraints on water column Zn isotope variability. In addition, the future collection of contemporaneous coral and seawater samples would enable a more direct comparison between fluid and solid compositions, thereby reducing uncertainties and improving the ability to test models of trace metal uptake and isotopic fractionation in corals.

The availability of local seawater Cu isotope data is much more limited than for Zn, which restricts us to a global-scale comparison between coralline and seawater $\delta^{65}Cu$ values. The average of the Holocene cold-water coral $\delta^{65}Cu$ dataset is +0.59 ± 0.23‰ (1SD, n = 15), comparable to the mean of published deep seawater $\delta^{65}Cu$ values, at +0.66 ± 0.09‰ (1SD, n = 119, all data >200m; Takano et al., 2014; Thompson and Ellwood, 2014; Little et al., 2018). However, there is considerably more variability in the coral $\delta^{65}Cu$ values, which range from +0.27 to +1.05‰, than is typically observed

in the deep ocean (Figs. 5, S4). Unless this variability reflects undiagnosed analytical artefacts (section 2.3), the presence of residual contaminating phases (which is not supported by mass balance calculations), or an influence from the chemical cleaning procedure (e.g., Yu et al., 2007; Druce, 2021), it suggests complexity in the mechanisms of Cu incorporation in coral aragonite.

Notably, the biogeochemistry of Cu and Cu isotopes, including Cu sorption and incorporation in calcite, is strongly influenced by organic complexation (McBride, 1981; Coale and Bruland, 1988; Lee et al., 2005; Ryan et al., 2014), and up to 2.5% by weight of live coral skeletons comprises organic material (plus associated water) (Cuif et al., 2004). It is interesting that the four coral specimens from the last glacial period are rather more homogeneous in their Cu isotope compositions (+0.66‰, +0.70‰, +0.73‰, +0.84‰) than the Holocene dataset, which could perhaps relate to the degradation of organics over time. However, we observe no relationship between coral age and δ^{65}Cu values for the Holocene and live-collected corals (Fig. S5), and so this hypothesis remains speculative. Further experimental, observational, and seawater Cu isotope analyses are required to better interpret the small dataset of cold-water coral Cu isotope compositions that is presented here as a starting point for any future endeavour.

4.3 Inorganic versus biogenic carbonate precipitation

For elemental ratios and isotopic compositions in carbonates to be useful paleoenvironmental tools, they should be free of so-called 'vital effects', or the impact of such vital effects should be systematic and quantifiable. This section considers in greater depth the possible inorganic controls and the influence of vital effects on coral Zn/Ca, Cu/Ca, δ^{66}Zn, and δ^{65}Cu values. We focus primarily on Zn because more information exists with which to evaluate the partitioning and isotope fractionation of Zn than Cu in carbonates.

4.3.1 Partitioning behaviour

Biogenic partition coefficients are not directly comparable to the thermodynamic framework developed for inorganic precipitation, because carbonate biomineralization is strongly organism-controlled (e.g., Elderfield et al., 1996). Foraminifera are thought to calcify via transmembrane transport and/or seawater vacuolization (De Nooijer et

668 al., 2014), while scleractinian corals calcify from a so-called 'extracellular calcifying
669 fluid' (ECF) (Adkins et al., 2003; Cohen and McConnaughey, 2003; Allemand et al.,
670 2004). Nevertheless, comparisons to inorganic systems can still be instructive.
671
672 Inorganic trace element partitioning experiments for calcium carbonates have focused
673 on calcite, in which Zn^{2+} and Cu^{2+} ions first adsorb on the mineral surface before
674 substituting isomorphously for octahedrally coordinated Ca^{2+} in the mineral structure
675 (Reeder et al., 1999; Elzinga and Reeder, 2002). The resulting inorganic partition
676 coefficients for Zn in calcite (see section 4.1) are generally high, ranging from ~5 to
677 >100 (Crocket and Winchester, 1966; Kitano et al., 1980; Rimstidt et al., 1998;
678 Temmam et al., 2000; Mavromatis et al., 2019). Using *ab initio* methods, Menadakis et
679 al. (2007, 2009) calculated that Zn^{2+} substitution for Ca^{2+} is more energetically
680 favourable in calcite than in aragonite, consistent with experimental results from Kitano
681 et al. (1973, 1980), which showed that Zn partition coefficients are a factor of 10 lower
682 for aragonite than for calcite (5 for aragonite cf. 50 for calcite). Fewer studies have
683 investigated Cu partitioning in carbonates, but estimated partition coefficients are in a
684 similar range to Zn (~20 – 80 for calcite; Kitano et al., 1980; Rimstidt et al., 1998) and
685 are also a factor of 10 lower for aragonite than calcite (e.g., 2.5 for aragonite cf. 25 for
686 calcite; Kitano et al., 1973). Such variability in inorganic partitioning likely reflects the
687 wide range of physical and chemical parameters, such as temperature, pressure, salinity,
688 metal concentration, pH, and calcite saturation state, that can all influence partitioning
689 behaviour (recently reviewed by Smrzka et al., 2019).
690
691 In culture, calcitic benthic foraminifera exhibit partition coefficients for both Zn and
692 Cu that are lower compared to inorganic values for calcite. Van Dijk et al. (2017)
693 calculated foraminiferal calcite D_{Zn} values of 0.7 to 1.9 (*Ammonia tepida*), and similar
694 values of 0.2 to 4.0 were estimated for *Pseudotriloculina rotunda* (Nardelli et al., 2016).
695 Munsel et al. (2010) determined a D_{Cu} value of 0.14 ± 0.02 for *A. tepida*, similar to the
696 estimate of 0.25 ± 0.15 for *A. tepida* and *Heteristegina depressa* (de Nooijer et al.,
697 2007). These low partition coefficients may in part be explained by the presence in the
698 culture media of other dissolved species such as Cl^- or organic complexes at higher
699 concentrations than in the inorganic experiments described above; both were shown to
700 reduce inorganic partitioning (Temmam et al., 2000; Lee et al., 2005). In addition, the
701 mechanism of incorporation may influence partitioning: active uptake of metals over a

membrane may be less favourable than sorption directly on the mineral surface in inorganic experiments (De Nooijer et al., 2014; van Dijk et al., 2017).

In the field, benthic foraminifera from ocean sediment core tops have estimated D_{Zn} values of ~9 (*Cibicidoides wuellerstorfi*; Marchitto et al., 2000) and ~22 (*Cibicidoides pachyderma*; Bryan and Marchitto, 2010), which are higher compared to cultured specimens but similar to the range observed in inorganic calcite experiments. Zinc partitioning in cultured foraminifera is also sensitive to Zn concentrations, with the highest partition coefficients arising at low Zn concentrations that are more comparable to natural seawater (Nardelli et al., 2016). Such an effect may explain the higher Zn partitioning in field-collected benthic foraminifera. Alternatively, or in addition, differences between field-collected and cultured foraminifera may result from species-specific vital effects, contamination of field-collected samples, or additional environmental controls on Zn incorporation (e.g., growth rate) (van Dijk et al., 2017).

Coral calcification occurs via the up-regulation of pH and aragonite saturation state in the ECF. This up-regulation is achieved via an enzymatic alkalinity pump (a Ca^{2+}-ATPase), which removes 2 protons for every Ca^{2+} ion pumped in (Ip et al., 1991; Al-Horani et al., 2003). As a result, dissolved inorganic carbon speciation shifts towards CO_3^{2-} and aragonite saturation state increases, which in turn aids aragonite precipitation. The observed partition coefficients for cold-water corals cover a wide range (Table 4), particularly those for Zn in *Caryophillia* (3.1 to 92), which span almost the entire range of measured inorganic and benthic foraminiferal values. We find no trace element evidence for residual contaminating phases (section 4.2) that could explain sporadic high D_{Zn} and D_{Cu} values. Instead, we suggest that the spread towards high values is a function of the high inorganic partition coefficients for Zn and Cu in aragonite coupled to variations in coral calcification efficiency.

Following Gagnon et al. (2012), calcification efficiency is defined as the balance between the supply of ions to the ECF from seawater and their removal via $CaCO_3$ precipitation. It can be viewed in terms of either a Rayleigh-type batch reactor (e.g., Gagnon et al., 2007) or a steady-state process (e.g., Gagnon et al., 2012), but the implications for elemental incorporation are similar. Aragonite that is precipitated near the start of a Rayleigh-type removal process, or in a well-flushed ECF reservoir (i.e.

low calcification efficiency), will have a high Zn/Ca or Cu/Ca value, reflecting the high inorganic partition coefficients of Zn and Cu. As calcification efficiency increases, either at steady state or following progressive Rayleigh distillation, Zn/Ca_{coral} and Cu/Ca_{coral} will approach seawater ratios, and therefore D values of one (grey dashed lines, Fig. 6). We speculate that the calcification efficiency of any individual specimen may reflect site- or species-specific differences. Furthermore, the variable partitioning behaviour observed for *Caryophyllia* may reflect the wide range of species diversity (at least 66 known species; Kitahara et al., 2010a).

4.3.2 Isotopic effects

There have been several experimental studies of Zn isotope fractionation during inorganic incorporation of Zn into or sorption onto carbonate minerals, though not specifically for aragonite. Dong and Wasylenki (2016) showed that the adsorption of Zn onto calcite is associated with a preference for heavy Zn isotopes, with $\Delta^{66}Zn_{CaCO3\text{-}solution}$ values (where $\Delta^{66}Zn_{CaCO3\text{-}solution} = \delta^{66}Zn_{CaCO3} - \delta^{66}Zn_{solution}$) of +0.4‰ to +0.7‰. They attribute this enrichment in heavy isotopes to a reduction in coordination number and Zn—O bond length on sorption of octahedrally coordinated Zn^{2+} aquo-complexes as tetrahedral surface complexes (Dong and Wasylenki, 2016). Smaller $\Delta^{66}Zn_{CaCO3\text{-}solution}$ values have generally been observed in co-precipitation experiments. Maréchal and Sheppard (2002) estimated a Zn isotope fractionation between smithsonite and fluid of <0.1‰, while Veeramani et al. (2015) found a small preference for light Zn isotopes on precipitation of hydrozincite (–0.18‰). However, Mavromatis et al. (2019) found that Zn isotope fractionation on co-precipitation with calcite is pH dependent, with $\Delta^{66}Zn_{CaCO3\text{-}solution}$ values in their experiments ranging from about 0‰ at pH 8.3 to +0.6‰ at pH 6.1. While not designed to replicate seawater chemistry exactly, their experimental results provide an important demonstration that aqueous Zn speciation and the isotopic fractionation between aqueous species need to be considered in order to explain carbonate $\delta^{66}Zn$ values.

In detail, Mavromatis et al. (2019) attributed the observed decrease in Zn isotope fractionation with increasing pH to an increase in the prevalence of aqueous $ZnHCO_3^+$ and $ZnCO_3^0$ relative to Zn^{2+}. Theoretical *ab initio* calculations predict that $ZnHCO_3^+$ and $ZnCO_3^0$ species are isotopically heavy compared to Zn^{2+}; therefore, the pool of Zn^{2+} is projected to get both smaller and isotopically lighter with increasing pH (Fujii

et al., 2014). Given that the Zn^{2+} species is incorporated into the calcite mineral structure (as a direct substitution for Ca^{2+}; Elzinga and Reeder, 2002; Elzinga et al., 2006), these changes in speciation should be reflected in the co-precipitation of calcite with a lighter Zn isotope composition and lower D_{Zn} value (Mavromatis et al., 2019). Such an affect does appear to be observed for D_{Zn} values in benthic foraminifera (van Dijk et al., 2017). Based on theoretical calculations, Mavromatis et al. (2019) also show that their experimental data are consistent with a constant offset between Zn in calcite and aqueous Zn^{2+} ($\Delta^{66}Zn_{calcite\text{-}Zn2+} = +0.6‰$) over the full pH range of their experiments. Following Dong and Wasylenki (2016), they attribute this enrichment of heavy Zn isotopes in the mineral phase (relative to aqueous Zn^{2+}) to isotope fractionation during Zn^{2+} *sorption* to the mineral surface (as per Elzinga and Reeder, 2002; Elzinga et al., 2006; Dong and Wasylenki, 2016), with its subsequent incorporation into the mineral structure proposed to occur without further isotope fractionation (Mavromatis et al., 2019).

In applying the above rationale to the organism-controlled calcification of cold-water corals, it is important to consider the up-regulation of pH in the ECF. Both direct observations (e.g., microsensor and pH-sensitive fluorescent dye) and indirect measurements (e.g., B isotopes) indicate up-regulation on the order of one pH unit above ambient seawater, to about pH 9 to 9.5 (e.g., Al-Horani et al., 2003; Rollion-Bard et al., 2011; Sevilgen et al., 2019). Using geochemical modelling, and also incorporating the effect of complexation of light Zn with the chloride ions found in seawater, Mavromatis et al. (2019) predict $\Delta^{66}Zn_{calcite\text{-}sw}$ values of about +0.3 to +0.4‰ for precipitation from 'inorganic seawater' at pH 9 to 9.5. Such a prediction clearly contrasts with the cold-water coral dataset presented here, for which $\Delta^{66}Zn_{coral\text{-}sw} \approx 0‰$.

However, Zn speciation in natural seawater (and, presumably, within coral ECF) is more complex than in those inorganic experiments, with a strong influence from complexation to dissolved organic ligands (e.g., Bruland, 1989; Ellwood and Van Den Berg, 2000; Jakuba et al., 2012). Dissolved organic ligands preferentially complex isotopically heavy Zn (Jouvin et al., 2009; Marković et al., 2017). Hence, it is plausible that the small residual Zn^{2+} pool in the ECF is isotopically lighter than would arise in inorganic-only scenarios, which would provide one means to reconcile the predictions of Mavromatis et al. (2019) with the cold-water coral dataset. If this scenario is correct,

804 it implies that our observation of $\Delta^{66}Zn_{coral\text{-}sw} \approx 0‰$ is fortuitous, reflecting the balance
805 between two approximately equal and opposite isotopic fractionations: one between
806 aqueous species (including organic ligands) in the ECF (driving Zn^{2+} to low $\delta^{66}Zn$
807 values), and the other linked to sorption of heavy Zn and its incorporation into coral
808 aragonite. As yet, while there are constraints on Zn sorption onto calcite, the mechanism
809 and Zn isotope fractionation of sorption and incorporation in aragonite is unknown.
810
811 Finally, variable coral calcification efficiency, suggested above as a means to explain
812 variable D_{Zn} (and D_{Cu}) values, may also have implications for coral Zn and Cu isotope
813 compositions. For example, if the isotope fractionation factor varies with aragonite
814 precipitation rate, or if a constant (non-zero) fractionation factor is combined with
815 calcification following a Rayleigh distillation trend, coral isotopic compositions should
816 evolve during calcification. However, in the data presented here, no clear trend is
817 resolved between Zn/Ca or Cu/Ca and their respective isotopic systems (Fig. 5). We
818 also observe that Zn/Ca ratios vary by a factor of two for cleaned sub-samples of the
819 glacial-age Sars Seamount coral, with no associated variability in $\delta^{66}Zn$ (Fig. 4). Taken
820 together, these observations support a small $\Delta^{66}Zn_{coral\text{-}sw}$ fractionation factor.
821
822 Overall, a rather complex picture emerges, in which aqueous speciation in the ECF, as
823 well as the mechanism of sorption and/or incorporation of Zn (and Cu) into aragonite,
824 could both play a role in determining coral isotopic compositions. Neither aspect is well
825 understood, and both merit further detailed study. It is noteworthy that the Zn isotope
826 compositions of diverse types of shallow water carbonates exhibit more variability
827 (-0.56 to +1.11‰; Zhao et al., 2021) than the data presented here, perhaps in part as a
828 result of the mechanisms outlined above. These authors also suggest kinetic effects as
829 a possible mechanism to explain the observed isotopic variability. As described above,
830 we do not see evidence for kinetic effects in the coral dataset, perhaps due to the slow
831 growth rates of cold-water corals (e.g., Adkins et al., 2004). A recent Zn isotope study
832 on shallow-water zooxanthellate corals also observed variability from ~0 to +0.6‰,
833 which they attributed to temperature and photosynthetic effects (Xiao et al., 2020),
834 neither of which are relevant factors for cold-water corals. Indeed, we find that cold-
835 water corals appear to reliably record seawater $\delta^{66}Zn$ values. Recommendations for
836 future work include expanding the cold-water coral sample set, micro-analytical studies

of spatial variability in individual corals, and experimental studies on isotopic fractionation in aragonite, both with and without organic ligands.

5. Conclusions and outlook for cold-water coral $\delta^{66}Zn$ values as a palaeoceanographic tracer

In summary, we show that thorough physical and chemical cleaning of cold-water corals effectively removes authigenic and detrital Zn- and Cu-containing phases, allowing isotopic analysis of the coral aragonite. We find significant interspecies variability in the partitioning behaviour of Zn and Cu in cold-water corals, and notable intra-specimen variability in Zn/Ca ratios. Aqueous speciation and coral calcification efficiency are considered likely drivers of this variability.

We focus on the palaeoceanographic potential of Zn isotope compositions in cold-water corals, due to the greater availability of seawater and experimental data in the literature for Zn compared to Cu. Somewhat unexpectedly given its variable partitioning behaviour, interspecies and intra-specimen Zn/Ca variability is not associated with variability in $\delta^{66}Zn$ values. To a first order, cold-water corals appear to record ambient seawater $\delta^{66}Zn$ values without isotope fractionation, suggesting their utility as an archive of past seawater Zn isotope compositions.

It is therefore conceivable that cold-water corals could be employed to trace past changes in whole oceanic Zn and Cu mass balance. In effect, cold-water corals from the intermediate and deep ocean record whole ocean isotopic compositions, given that the deep ocean is largely isotopically homogeneous (at least in the modern day) and contains over 95% of the total oceanic Zn inventory. At steady state, the whole ocean isotopic composition is a balance of the isotopic composition of the inputs ($\delta^{66}Zn_{input}$) and any isotopic fractionation on output to sediments (Δ_{output}):

$$\delta^{66}Zn_{ocean} = \delta^{66}Zn_{input} - \Delta_{output} \quad (8)$$

The major sedimentary output fluxes for Zn are Fe-Mn (hydr)oxides and organic-rich sediments (Little et al., 2014, 2016), whereas removal to carbonates is negligible and does not significantly impact the oceanic mass balance. As a result, Zn isotope compositions of cold-water corals should reflect changes in whole ocean Zn cycling on

timescales comparable to its ocean residence time (estimated Zn τ_{res} = 3–8 kyr, Little et al., 2016; Roshan et al., 2016).

The dataset of Zn and Cu isotopes on glacial-age corals presented here comprises only four samples, which precludes firm interpretations. Nonetheless, their δ^{66}Zn and δ^{65}Cu values generally overlap with Holocene corals and modern seawater from their respective settings, suggesting only limited glacial-interglacial changes in the deep ocean Zn and Cu budgets. It is notable, however, that the two North Atlantic corals have more positive δ^{66}Zn values (+0.79‰, +0.67‰) than the corals from the Southern Ocean and the Tasman Sea (+0.37‰, +0.38‰), hinting at past spatial variability, such as a possible change in the isotopic composition of the northern-sourced water mass endmember on glacial-interglacial timescales.

Finally, we emphasise that archives from shallow water depths are likely to be most sensitive to recording past changes in oceanic Zn cycling. The pioneering study of Pichat et al. (2003) analysed δ^{66}Zn values in the leachable carbonate fraction of a Pacific sediment core spanning the last 180 kyr. This record exhibits high frequency variability and a long-term trend towards lighter Zn isotope compositions over this interval (Pichat et al., 2003). Since the sediment core is primarily made up of coccoliths, these variations were interpreted in terms of changes in the Zn isotope composition of the surface ocean. By constraining any past changes in the whole ocean mass balance of Zn, a comparable cold-water coral record from deeper water depths would aid in the interpretation of such surface water variability. Future cold-water coral studies with better spatial and temporal coverage should enable a more detailed investigation of past changes in the oceanic Zn cycle.

Acknowledgements

We would like to acknowledge Matthew Clarkson and an anonymous reviewer for thoughtful comments on a previous version of this manuscript. Many thanks to Katharina Kreissig and Barry Coles for maintaining the smooth running of the MAGIC labs at Imperial, and to Derek Vance for the use of the Neptune at ETH. Thanks also to Sophie Hines, who sub-sampled New England Seamount corals from the Adkins collection. Finally, thanks to Tristan Horner, who provided valuable insights early on

in the development of this project. This research was supported by a Leverhulme Trust early career fellowship to SHL (ECF-2014-615). DJW and TvdF acknowledge support from the Natural Environment Research Council (NE/N001141/1) and a NERC independent research fellowship (NE/T011440/1). SHL is currently supported by a NERC independent research fellowship (NE/P018181/2).

References

Adkins, J.F., Boyle, E.A., Curry, W.B., Lutringer, A., 2003. Stable isotopes in deep-sea corals and a new mechanism for "vital effects." Geochim. Cosmochim. Acta. https://doi.org/10.1016/S0016-7037(00)01203-6

Adkins, J.F., Henderson, G.M., Wang, S.-L., O'Shea, S., Mokadem, F., 2004. Growth rates of the deep-sea scleractinia Desmophyllum cristagalli and Enallopsammia rostrata. Earth Planet. Sci. Lett. 227, 481–490.

Al-Horani, F.A., Al-Moghrabi, S.M., De Beer, D., 2003. The mechanism of calcification and its relation to photosynthesis and respiration in the scleractinian coral Galaxea fascicularis. Mar. Biol. 142, 419–426.

Albarède, F., 2004. The Stable Isotope Geochemistry of Copper and Zinc. Rev. Mineral. Geochemistry 55, 409–427. https://doi.org/http://dx.doi.org/10.2138/gsrmg.55.1.409

Allemand, D., Ferrier-Pagès, C., Furla, P., Houlbrèque, F., Puverel, S., Reynaud, S., Tambutté, É., Tambutté, S., Zoccola, D., 2004. Biomineralisation in reef-building corals: From molecular mechanisms to environmental control. Comptes Rendus - Palevol 3, 453–467. https://doi.org/10.1016/j.crpv.2004.07.011

Anagnostou, E., Sherrell, R.M., Gagnon, A., LaVigne, M., Field, M.P., McDonough, W.F., 2011. Seawater nutrient and carbonate ion concentrations recorded as P/Ca, Ba/Ca, and U/Ca in the deep-sea coral Desmophyllum dianthus. Geochim. Cosmochim. Acta 75, 2529–2543. https://doi.org/10.1016/j.gca.2011.02.019

Andersen, M.B., Vance, D., Archer, C., Anderson, R.F., Ellwood, M.J., Allen, C.S., 2011. The Zn abundance and isotopic composition of diatom frustules, a proxy for Zn availability in ocean surface seawater. Earth Planet. Sci. Lett. 301, 137–145. https://doi.org/10.1016/j.epsl.2010.10.032

Archer, C., Vance, D., 2004. Mass discrimination correction in multiple-collector plasma source mass spectrometry: an example using Cu and Zn isotopes. J. Anal. At. Spectrom. 19, 656. https://doi.org/10.1039/b315853e

939 Arnold, T., Schönbächler, M., Rehkämper, M., Dong, S., Zhao, F.J., Kirk, G.J.D.,
940 Coles, B.J., Weiss, D.J., 2010. Measurement of zinc stable isotope ratios in
941 biogeochemical matrices by double-spike MC-ICPMS and determination of the
942 isotope ratio pool available for plants from soil. Anal. Bioanal. Chem. 398,
943 3115–3125. https://doi.org/10.1007/s00216-010-4231-5
944 Baconnais, I., Rouxel, O., Dulaquais, G., Boye, M., 2019. Determination of the
945 copper isotope composition of seawater revisited: A case study from the
946 Mediterranean Sea. Chem. Geol. 511, 465–480.
947 https://doi.org/10.1016/j.chemgeo.2018.09.009
948 Bigalke, M., Weyer, S., Kobza, J., Wilcke, W., 2010. Stable Cu and Zn isotope ratios
949 as tracers of sources and transport of Cu and Zn in contaminated soil. Geochim.
950 Cosmochim. Acta 74, 6801–6813. https://doi.org/10.1016/j.gca.2010.08.044
951 Boyle, E.A., 1981. Cadmium, zinc, copper, and barium in foraminifera tests. Earth
952 Planet. Sci. Lett. 53, 11–35. https://doi.org/10.1016/0012-821X(81)90022-4
953 Boyle, E.A., Sclater, F.R., Edmond, J.M., 1977. The distribution of dissolved copper
954 in the Pacific. Earth Planet. Sci. Lett. 37, 38–54. https://doi.org/10.1016/0012-
955 821X(77)90144-3
956 Brahmi, C., Kopp, C., Domart-Coulon, I., Stolarski, J., Meibom, A., 2012. Skeletal
957 growth dynamics linked to trace-element composition in the scleractinian coral
958 Pocillopora damicornis. Geochim. Cosmochim. Acta 99, 146–158.
959 Bridgestock, L.J., Williams, H., Rehkämper, M., Larner, F., Giscard, M.D.,
960 Hammond, S., Coles, B., Andreasen, R., Wood, B.J., Theis, K.J., 2014.
961 Unlocking the zinc isotope systematics of iron meteorites. Earth Planet. Sci. Lett.
962 400, 153–164.
963 Bruland, K.W., 1989. Complexation of zinc by natural organic ligands in the central
964 North Pacific. Limnol. Oceanogr. 34, 269–285.
965 Bruland, K.W., 1980. Oceanographic distributions of cadmium, zinc, nickel and
966 copper in the North Pacific. Earth Planet. Sci. Lett. 47, 176–198.
967 Bruland, K.W., Middag, R., Lohan, M.C., 2013. Controls of Trace Metals in
968 Seawater, 2nd ed, Treatise on Geochemistry: Second Edition. Elsevier Ltd.
969 https://doi.org/10.1016/B978-0-08-095975-7.00602-1
970 Bryan, S.P., Marchitto, T.M., 2010. Testing the utility of paleonutrient proxies Cd/Ca
971 and Zn/Ca in benthic foraminifera from thermocline waters. Geochemistry,
972 Geophys. Geosystems 11, n/a-n/a. https://doi.org/10.1029/2009GC002780

973 Brzezinski, M.A., Pride, C.J., Franck, V.M., Sigman, D.M., Sarmiento, J.L.,
974 Matsumoto, K., Gruber, N., Rau, G.H., Coale, K.H., 2002. A switch from Si
975 (OH) 4 to NO3− depletion in the glacial Southern Ocean. Geophys. Res. Lett.
976 29, 1–5.
977 Burke, A., 2012. Constraining Circulation Changes Through the Last Deglaciation
978 with Deep-sea Coral Radiocarbon and Sedimentary 231Pa/230Th. MIT/WHOI.
979 Case, D.H., Robinson, L.F., Auro, M.E., Gagnon, A.C., 2010. Environmental and
980 biological controls on Mg and Li in deep-sea scleractinian corals. Earth Planet.
981 Sci. Lett. 300, 215–225. https://doi.org/10.1016/j.epsl.2010.09.029
982 Chen, T., Robinson, L.F., Beasley, M.P., Claxton, L.M., Andersen, M.B., Gregoire,
983 L.J., Wadham, J., Fornari, D.J., Harpp, K.S., 2016. Ocean mixing and ice-sheet
984 control of seawater 234U/238U during the last deglaciation. Science (80-.).
985 https://doi.org/10.1126/science.aag1015
986 Chen, T., Robinson, L.F., Burke, A., Southon, J., Spooner, P., Morris, P.J., Ng, H.C.,
987 2015. Synchronous centennial abrupt events in the ocean and atmosphere during
988 the last deglaciation. Science (80-.). https://doi.org/10.1126/science.aac6159
989 Cheng, H., Adkins, J., Edwards, R.L., Boyle, E.A., 2000. U-Th dating of deep-sea
990 corals. Geochim. Cosmochim. Acta 64, 2401–2416.
991 https://doi.org/10.1016/S0016-7037(99)00422-6
992 Clarkson, M.O., Müsing, K., Andersen, M.B., Vance, D., 2020. Examining pelagic
993 carbonate-rich sediments as an archive for authigenic uranium and molybdenum
994 isotopes using reductive cleaning and leaching experiments. Chem. Geol. 539,
995 119412. https://doi.org/10.1016/j.chemgeo.2019.119412
996 Coale, K.H., Bruland, K.W., 1988. Copper complexation in the Northest Pacific.
997 Limnol. Oceanogr. 33, 1084–1101.
998 Cohen, A.L., McConnaughey, T.A., 2003. Geochemical Perspectives on Coral
999 Mineralization. Rev. Mineral. Geochemistry 54, 151–187.
1000 https://doi.org/10.2113/0540151
1001 Conway, T.M., John, S.G., 2015. The cycling of iron, zinc and cadmium in the North
1002 East Pacific Ocean - Insights from stable isotopes. Geochim. Cosmochim. Acta
1003 164, 262–283. https://doi.org/10.1016/j.gca.2015.05.023
1004 Conway, T.M., John, S.G., 2014. The biogeochemical cycling of zinc and zinc
1005 isotopes in the North Atlantic Ocean. Global Biogeochem. Cycles 1111–1128.
1006 https://doi.org/10.1002/2014GB004862.Received

1007 Crocket, J.H., Winchester, J.W., 1966. Coprecipitation of zinc with calcium
1008 carbonate. Geochim. Cosmochim. Acta 30, 1093–1109.
1009 https://doi.org/10.1016/0016-7037(66)90119-0
1010 Crocket, K.C., Lambelet, M., van de Flierdt, T., Rehkämper, M., Robinson, L.F.,
1011 2014. Measurement of fossil deep-sea coral Nd isotopic compositions and
1012 concentrations by TIMS as NdO+, with evaluation of cleaning protocols. Chem.
1013 Geol. 374–375, 128–140. https://doi.org/10.1016/j.chemgeo.2014.03.011
1014 Cuif, J.-P., Dauphin, Y., Doucet, J., Salome, M., Susini, J., 2003. XANES mapping of
1015 organic sulfate in three scleractinian coral skeletons. Geochim. Cosmochim.
1016 Acta 67, 75–83.
1017 Cuif, J.P., Dauphin, Y., Berthet, P., Jegoudez, J., 2004. Associated water and organic
1018 compounds in coral skeletons: Quantitative thermogravimetry coupled to
1019 infrared absorption spectrometry. Geochemistry, Geophys. Geosystems 5, 1–9.
1020 https://doi.org/10.1029/2004GC000783
1021 de Nooijer, L.J., Reichart, G.J., Dueñas-Bohórquez, A., Wolthers, M., Ernst, S.R.,
1022 Mason, P.R.D., van der Zwaan, G.J., 2007. Copper incorporation in
1023 foraminiferal calcite: results from culturing experiments. Biogeosciences
1024 Discuss. 4, 961–991. https://doi.org/10.5194/bgd-4-961-2007
1025 De Nooijer, L.J., Spero, H.J., Erez, J., Bijma, J., Reichart, G.J., 2014.
1026 Biomineralization in perforate foraminifera. Earth-Science Rev.
1027 https://doi.org/10.1016/j.earscirev.2014.03.013
1028 de Souza, G.F., Khatiwala, S.P., Hain, M.P., Little, S.H., Vance, D., 2018. On the
1029 origin of the marine zinc–silicon correlation. Earth Planet. Sci. Lett. 492, 22–34.
1030 https://doi.org/10.1016/j.epsl.2018.03.050
1031 Dong, S., Wasylenki, L.E., 2016. Zinc isotope fractionation during adsorption to
1032 calcite at high and low ionic strength. Chem. Geol. 447, 70–78.
1033 Druce, M., 2021. Expanding the utility of the zinc and cadmium stable isotope
1034 micronutrient proxies, and reconstructing palaeo-productivity through the last
1035 deglaciation. University of Otago.
1036 Elderfield, H., Bertram, C.J., Erez, J., 1996. A biomineralization model for the
1037 incorporation of trace elements into foraminiferal calcium carbonate. Earth
1038 Planet. Sci. Lett. 142, 409–423. https://doi.org/10.1016/0012-821x(96)00105-7
1039 Ellwood, M.J., Van Den Berg, C.M.G., 2000. Zinc speciation in the Northeastern
1040 Atlantic Ocean. Mar. Chem. 68, 295–306. https://doi.org/10.1016/S0304-

4203(99)00085-7
Elzinga, E.J., Reeder, R.J., 2002. X-ray absorption spectroscopy study of Cu2+ and Zn2+ adsorption complexes at the calcite surface: Implications for site-specific metal incorporation preferences during calcite crystal growth. Geochim. Cosmochim. Acta 66, 3943–3954. https://doi.org/10.1016/S0016-7037(02)00971-7
Elzinga, E.J., Rouff, A.A., Reeder, R.J., 2006. The long-term fate of Cu2+, Zn2+, and Pb2+ adsorption complexes at the calcite surface: An X-ray absorption spectroscopy study. Geochim. Cosmochim. Acta 70, 2715–2725. https://doi.org/10.1016/j.gca.2006.02.026
Finch, A.A., Allison, N., 2008. Mg structural state in coral aragonite and implications for the paleoenvironmental proxy. Geophys. Res. Lett. 35.
Fujii, T., Moynier, F., Blichert-Toft, J., Albarède, F., 2014. Density functional theory estimation of isotope fractionation of Fe, Ni, Cu, and Zn among species relevant to geochemical and biological environments. Geochim. Cosmochim. Acta 140, 553–576. https://doi.org/10.1016/j.gca.2014.05.051
Gabitov, R.I., Gaetani, G.A., Watson, E.B., Cohen, A.L., Ehrlich, H.L., 2008. Experimental determination of growth rate effect on U6+ and Mg2+ partitioning between aragonite and fluid at elevated U6+ concentration. Geochim. Cosmochim. Acta 72, 4058–4068.
Gagnon, A.C., Adkins, J.F., Erez, J., 2012. Seawater transport during coral biomineralization. Earth Planet. Sci. Lett. 329–330, 150–161. https://doi.org/10.1016/j.epsl.2012.03.005
Gagnon, A.C., Adkins, J.F., Fernandez, D.P., Robinson, L.F., 2007. Sr/Ca and Mg/Ca vital effects correlated with skeletal architecture in a scleractinian deep-sea coral and the role of Rayleigh fractionation. Earth Planet. Sci. Lett. 261, 280–295. https://doi.org/10.1016/j.epsl.2007.07.013
Hasenfratz, A.P., Martínez-García, A., Jaccard, S.L., Vance, D., Wälle, M., Greaves, M., Haug, G.H., 2017. Determination of the Mg/Mn ratio in foraminiferal coatings: An approach to correct Mg/Ca temperatures for Mn-rich contaminant phases. Earth Planet. Sci. Lett. 457, 335–347. https://doi.org/10.1016/j.epsl.2016.10.004
Hemsing, F., Hsieh, Y.-T., Bridgestock, L., Spooner, P.T., Robinson, L.F., Frank, N., Henderson, G.M., 2018. Barium isotopes in cold-water corals. Earth Planet. Sci.

Lett. 491, 183–192.
Hendry, K.R., Andersen, M.B., 2013. The zinc isotopic composition of siliceous marine sponges: Investigating nature's sediment traps. Chem. Geol. 354, 33–41. https://doi.org/10.1016/j.chemgeo.2013.06.025
Ip, Y.K., Lim, A.L.L., Lim, R.W.L., 1991. Some properties of calcium-activated adenosine triphosphatase from the hermatypic coralGalaxea fascicularis. Mar. Biol. 111, 191–197.
Jakuba, R.W., Saito, M.A., Moffett, J.W., Xu, Y., 2012. Dissolved zinc in the subarctic North Pacific and Bering Sea: Its distribution, speciation, and importance to primary producers. Global Biogeochem. Cycles 26, 1–15. https://doi.org/10.1029/2010GB004004
John, S.G., Conway, T.M., 2014. A role for scavenging in the marine biogeochemical cycling of zinc and zinc isotopes. Earth Planet. Sci. Lett. 394, 159–167. https://doi.org/10.1016/j.epsl.2014.02.053
John, S.G., Geis, R.W., Saito, M.A., Boyle, E.A., 2007. Zinc isotope fractionation during high affinity and low-affinity zinc transport by the marine diatom Thalassiosire oceanica. Limnol. Oceanogr. 52, 2710–2714.
John, S.G., Helgoe, J., Townsend, E., 2018. Biogeochemical cycling of Zn and Cd and their stable isotopes in the Eastern Tropical South Pacific. Mar. Chem. 201, 256–262. https://doi.org/10.1016/j.marchem.2017.06.001
John, S.G., Kunzmann, M., Townsend, E.J., Rosenberg, A.D., 2017. Zinc and cadmium stable isotopes in the geological record: A case study from the post-snowball Earth Nuccaleena cap dolostone. Palaeogeogr. Palaeoclimatol. Palaeoecol. 466, 202–208. https://doi.org/10.1016/j.palaeo.2016.11.003
Jouvin, D., Louvat, P., Juillot, F., Maréchal, C.N., Benedetti, M.F., 2009. Zinc isotopic fractionation: Why organic matters. Environ. Sci. Technol. 43, 5747–5754. https://doi.org/10.1021/es803012e
Kitahara, M. V, Cairns, S.D., Miller, D.J., 2010a. Monophyletic origin of Caryophyllia (Scleractinia, Caryophylliidae), with descriptions of six new species. Syst. Biodivers. 8, 91–118.
Kitahara, M. V, Cairns, S.D., Stolarski, J., Blair, D., Miller, D.J., 2010b. A comprehensive phylogenetic analysis of the Scleractinia (Cnidaria, Anthozoa) based on mitochondrial CO1 sequence data. PLoS One 5.
Kitano, Y., Kanamori, N., Tokuyama, A., Comori, T., 1973. Factors controlling the

1109 trace-element contents of marine carbonate skeletons, in: Proceeding of
1110 Symposium on Hydrogeochemistry and Biogeochemistry, The Clarke Co,
1111 Washington, DC. pp. 484–499.
1112 Kitano, Y., Okumura, M., Idogaki, M., 1980. Abnormal behaviors of copper (II) and
1113 zinc ions in parent solution at the early stage of calcite formation. Geochem. J.
1114 14, 167–175. https://doi.org/10.2343/geochemj.14.167
1115 Köbberich, M., Vance, D., 2017. Kinetic control on Zn isotope signatures recorded in
1116 marine diatoms. Geochim. Cosmochim. Acta 210, 97–113.
1117 https://doi.org/10.1016/j.gca.2017.04.014
1118 Kunzmann, M., Halverson, G.P., Sossi, P.A., Raub, T.D., Payne, J.L., Kirby, J., 2013.
1119 Zn isotope evidence for immediate resumption of primary productivity after
1120 snowball Earth. Geology 41, 27–30. https://doi.org/10.1130/G33422.1
1121 Lee, Y.J., Elzinga, E.J., Reeder, R.J., 2005. Cu(II) adsorption at the calcite-water
1122 interface in the presence of natural organic matter: Kinetic studies and
1123 molecular-scale characterization. Geochim. Cosmochim. Acta 69, 49–61.
1124 https://doi.org/10.1016/j.gca.2004.06.015
1125 Lemaitre, N., de Souza, G.F., Archer, C., Wang, R.M., Planquette, H., Sarthou, G.,
1126 Vance, D., 2020. Pervasive sources of isotopically light zinc in the North
1127 Atlantic Ocean. Earth Planet. Sci. Lett. 539, 116216.
1128 https://doi.org/10.1016/j.epsl.2020.116216
1129 Liao, W.H., Takano, S., Yang, S.C., Huang, K.F., Sohrin, Y., Ho, T.Y., 2020. Zn
1130 Isotope Composition in the Water Column of the Northwestern Pacific Ocean:
1131 The Importance of External Sources. Global Biogeochem. Cycles 34, 1–18.
1132 https://doi.org/10.1029/2019GB006379
1133 Little, S.H., Archer, C., Milne, A., Schlosser, C., Achterberg, E.P., Lohan, M.C.,
1134 Vance, D., 2018. Paired dissolved and particulate phase Cu isotope distributions
1135 in the South Atlantic. Chem. Geol. 502, 29–43.
1136 https://doi.org/10.1016/j.chemgeo.2018.07.022
1137 Little, S.H., Munson, S., Prytulak, J., Coles, B.J., Hammond, S.J., Widdowson, M.,
1138 2019. Cu and Zn isotope fractionation during extreme chemical weathering.
1139 Geochim. Cosmochim. Acta 263, 85–107.
1140 https://doi.org/10.1016/j.gca.2019.07.057
1141 Little, S.H., Vance, D., McManus, J., Severmann, S., 2016. Key role of continental
1142 margin sediments in the oceanic mass balance of Zn and Zn isotopes. Geology

1143 44, 207–210. https://doi.org/10.1130/G37493.1
1144 Little, S.H., Vance, D., McManus, J., Severmann, S., Lyons, T.W., 2017. Copper
1145 isotope signatures in modern marine sediments. Geochim. Cosmochim. Acta
1146 212, 253–273. https://doi.org/10.1016/j.gca.2017.06.019
1147 Little, S.H., Vance, D., Siddall, M., Gasson, E., 2013. A modeling assessment of the
1148 role of reversible scavenging in controlling oceanic dissolved Cu and Zn
1149 distributions. Global Biogeochem. Cycles 27, 780–791.
1150 https://doi.org/10.1002/gbc.20073
1151 Little, S.H., Vance, D., Walker-Brown, C., Landing, W.M., 2014. The oceanic mass
1152 balance of copper and zinc isotopes, investigated by analysis of their inputs, and
1153 outputs to ferromanganese oxide sediments. Geochim. Cosmochim. Acta 125,
1154 673–693. https://doi.org/10.1016/j.gca.2013.07.046
1155 Liu, S.A., Wu, H., Shen, S.Z., Jiang, G., Zhang, S., Lv, Y., Zhang, H., Li, S., 2017.
1156 Zinc isotope evidence for intensive magmatism immediately before the end-
1157 Permian mass extinction. Geology 45, 343–346.
1158 https://doi.org/10.1130/G38644.1
1159 Lomitschka, M., Mangini, A., 1999. Precise Th/U-dating of small and heavily coated
1160 samples of deep sea corals. Earth Planet. Sci. Lett. 170, 391–401.
1161 https://doi.org/10.1016/S0012-821X(99)00117-X
1162 Marchitto, T.M., Broecker, W.S., 2006. Deep water mass geometry in the glacial
1163 Atlantic Ocean: A review of constraints from the paleonutrient proxy Cd/Ca.
1164 Geochemistry, Geophys. Geosystems 7. https://doi.org/10.1029/2006GC001323
1165 Marchitto, T.M., Curry, W.B., Oppo, D.W., 2000. Zinc concentrations in benthic
1166 foraminifera reflect seawater chemistry. Paleoceanography 15, 299–306.
1167 Marchitto, T.M., Lynch-Stieglitz, J., Hemming, S.R., 2005. Deep Pacific CaCO3
1168 compensation and glacial-interglacial atmospheric CO2. Earth Planet. Sci. Lett.
1169 231, 317–336. https://doi.org/10.1016/j.epsl.2004.12.024
1170 Marechal, C., Sheppard, S., 2002. Isotopic fractionation of Cu and Zn between
1171 chloride and nitrate solutions and malachite or smithsonite at 30 degrees and 50
1172 degrees. Geochim. Cosmochim. Acta 66, A484–A484.
1173 Maréchal, C.N., Nicolas, E., Douchet, C., Albarède, F., 2000. Abundance of zinc
1174 isotopes as a marine biogeochemical tracer. Geochemistry, Geophys.
1175 Geosystems 1, n/a-n/a. https://doi.org/10.1029/1999GC000029
1176 Maréchal, C.N., Télouk, P., Albarède, F., 1999. Precise analysis of copper and zinc

isotopic compositions by plasma-source mass spectrometry. Chem. Geol. 156, 251–273. https://doi.org/10.1016/S0009-2541(98)00191-0

Margolin, A.R., Robinson, L.F., Burke, A., Waller, R.G., Scanlon, K.M., Roberts, M.L., Auro, M.E., van de Flierdt, T., 2014. Temporal and spatial distributions of cold-water corals in the Drake Passage: Insights from the last 35,000 years. Deep. Res. Part II Top. Stud. Oceanogr. 99, 237–248. https://doi.org/10.1016/j.dsr2.2013.06.008

Marković, T., Manzoor, S., Humphreys-Williams, E., Kirk, G.J.D., Vilar, R., Weiss, D.J., 2017. Experimental Determination of Zinc Isotope Fractionation in Complexes with the Phytosiderophore 2′-Deoxymugeneic Acid (DMA) and Its Structural Analogues, and Implications for Plant Uptake Mechanisms. Environ. Sci. Technol. 51, 98–107. https://doi.org/10.1021/acs.est.6b00566

Matsumoto, K., Sarmiento, J.L., Brzezinski, M.A., 2002. Silicic acid leakage from the Southern Ocean: A possible explanation for glacial atmospheric pCO2. Global Biogeochem. Cycles 16, 1–5.

Mavromatis, V., González, A.G., Dietzel, M., Schott, J., 2019. Zinc isotope fractionation during the inorganic precipitation of calcite – Towards a new pH proxy. Geochim. Cosmochim. Acta 244, 99–112. https://doi.org/10.1016/j.gca.2018.09.005

McBride, M.B., 1981. Forms and distribution of copper in solid and solution phases of soil, in: Loneragan, J.F., Robson, A.D., Graham, R.D. (Eds.), Copper in Soils and Plants. Academic Press: Australia.

Meibom, A., Cuif, J.P., Houlbreque, F., Mostefaoui, S., Dauphin, Y., Meibom, K.L., Dunbar, R., 2008. Compositional variations at ultra-structure length scales in coral skeleton. Geochim. Cosmochim. Acta 72, 1555–1569. https://doi.org/10.1016/j.gca.2008.01.009

Menadakis, M., Maroulis, G., Koutsoukos, P.G., 2009. Incorporation of Mg2+, Sr2+, Ba2+and Zn2+into aragonite and comparison with calcite. J. Math. Chem. 46, 484–491. https://doi.org/10.1007/s10910-008-9490-4

Menadakis, M., Maroulis, G., Koutsoukos, P.G., 2007. A quantum chemical study of doped CaCO3 (calcite). Comput. Mater. Sci. 38, 522–525.

Middag, R., de Baar, H.J.W., Bruland, K.W., 2019. The Relationships Between Dissolved Zinc and Major Nutrients Phosphate and Silicate Along the GEOTRACES GA02 Transect in the West Atlantic Ocean. Global Biogeochem.

Cycles. https://doi.org/10.1029/2018GB006034
Moffett, J.W., Dupont, C., 2007. Cu complexation by organic ligands in the sub-arctic NW Pacific and Bering Sea. Deep Sea Res. Part I Oceanogr. Res. Pap. 54, 586–595. https://doi.org/10.1016/j.dsr.2006.12.013
Moynier, F., Vance, D., Fujii, T., Savage, P., 2017. The Isotope Geochemistry of Zinc and Copper. Rev. Mineral. Geochemistry 82, 543–600. https://doi.org/10.2138/rmg.2017.82.13
Munsel, D., Kramar, U., Dissard, D., Nehrke, G., Berner, Z., Bijma, J., Reichart, G.-J., Neumann, T., 2010. Heavy metal uptake in foraminiferal calcite: results of multi-element culture experiments. Biogeosciences Discuss. 7, 953–977. https://doi.org/10.5194/bgd-7-953-2010
Nardelli, M.P., Malferrari, D., Ferretti, A., Bartolini, A., Sabbatini, A., Negri, A., 2016. Zinc incorporation in the miliolid foraminifer Pseudotriloculina rotunda under laboratory conditions. Mar. Micropaleontol. 126, 42–49. https://doi.org/10.1016/j.marmicro.2016.06.001
Pichat, S., Douchet, C., Albarède, F., 2003. Zinc isotope variations in deep-sea carbonates from the eastern equatorial Pacific over the last 175 ka. Earth Planet. Sci. Lett. 210, 167–178. https://doi.org/10.1016/S0012-821X(03)00106-7
Pratt, N., Chen, T., Li, T., Wilson, D.J., van de Flierdt, T., Little, S.H., Taylor, M.L., Robinson, L.F., Rogers, A.D., Santodomingo, N., 2019. Temporal distribution and diversity of cold-water corals in the southwest Indian Ocean over the past 25,000 years. Deep. Res. Part I Oceanogr. Res. Pap. 149. https://doi.org/10.1016/j.dsr.2019.05.009
Reeder, R.J., Lamble, G.M., Northrup, P.A., 1999. XAFS study of the coordination and local relaxation around Co2+, Zn2+, Pb2+, and Ba2+ trace elements in calcite. Am. Mineral. 84, 1049–1060.
Richon, C., Tagliabue, A., 2019. Insights Into the Major Processes Driving the Global Distribution of Copper in the Ocean From a Global Model. Global Biogeochem. Cycles 33, 1594–1610. https://doi.org/10.1029/2019GB006280
Rimstidt, J.D., Balog, A., Webb, J., 1998. Distribution of trace elements between carbonate minerals and aqueous solutions. Geochim. Cosmochim. Acta 62, 1851–1863. https://doi.org/10.1016/s0016-7037(98)00125-2
Roberts, J.M., Wheeler, A., Freiwald, A., Cairns, S., 2009. Cold-water corals: the biology and geology of deep-sea coral habitats. Cambridge University Press.

1245 Robinson, L.F., Adkins, J., Scheirer, D., Fernandez, D.P., Gagnon, a C., Waller, R.,
1246 2007. Deep-sea scleractinian coral age and depth distributions in the NW
1247 Atlantic for the last 225 thousand years. Bull. Mar. Sci. 81, 371–391.
1248 Robinson, L.F., Adkins, J.F., Frank, N., Gagnon, A.C., Prouty, N.G., Brendan Roark,
1249 E., de Flierdt, T. van, 2014. The geochemistry of deep-sea coral skeletons: A
1250 review of vital effects and applications for palaeoceanography. Deep. Res. Part II
1251 Top. Stud. Oceanogr. 99, 184–198. https://doi.org/10.1016/j.dsr2.2013.06.005
1252 Rollion-Bard, C., Blamart, D., Cuif, J.-P., Dauphin, Y., 2010. In situ measurements of
1253 oxygen isotopic composition in deep-sea coral, Lophelia pertusa: Re-
1254 examination of the current geochemical models of biomineralization. Geochim.
1255 Cosmochim. Acta 74, 1338–1349.
1256 Rollion-Bard, C., Blamart, D., Trebosc, J., Tricot, G., Mussi, A., Cuif, J.-P., 2011.
1257 Boron isotopes as pH proxy: A new look at boron speciation in deep-sea corals
1258 using 11B MAS NMR and EELS. Geochim. Cosmochim. Acta 75, 1003–1012.
1259 https://doi.org/https://doi.org/10.1016/j.gca.2010.11.023
1260 Roshan, S., Wu, J., 2015. The distribution of dissolved copper in the tropical-
1261 subtropical north Atlantic across the GEOTRACES GA03 transect. Mar. Chem.
1262 176, 189–198. https://doi.org/10.1016/j.marchem.2015.09.006
1263 Roshan, S., Wu, J., Jenkins, W.J., 2016. Long-range transport of hydrothermal
1264 dissolved Zn in the tropical South Pacific. Mar. Chem. 183, 25–32.
1265 https://doi.org/10.1016/j.marchem.2016.05.005
1266 Ryan, B.M., Kirby, J.K., Degryse, F., Scheiderich, K., McLaughlin, M.J., 2014.
1267 Copper isotope fractionation during equilibration with natural and synthetic
1268 ligands. Environ. Sci. Technol. 48, 8620–8626.
1269 https://doi.org/10.1021/es500764x
1270 Samanta, M., Ellwood, M.J., Sinoir, M., Hassler, C.S., 2017. Dissolved zinc isotope
1271 cycling in the Tasman Sea, SW Pacific Ocean. Mar. Chem. 192, 1–12.
1272 https://doi.org/10.1016/j.marchem.2017.03.004
1273 Sarmiento, J.L., Gruber, N., Brzezinski, M.A., Dunne, J.P., 2004. High-latitude
1274 controls of thermocline nutrients and low latitude biological productivity. Nature
1275 427, 56–60.
1276 Schlitzer, R., Anderson, R.F., Dodas, E.M., Lohan, M., Geibert, W., Tagliabue, A.,
1277 Bowie, A., Jeandel, C., Maldonado, M.T., Landing, W.M., Cockwell, D.,
1278 Abadie, C., Abouchami, W., Achterberg, E.P., Agather, A., Aguliar-Islas, A.,

van Aken, H.M., Andersen, M., Archer, C., Auro, M., de Baar, H.J., Baars, O., Baker, A.R., Bakker, K., Basak, C., Baskaran, M., Bates, N.R., Bauch, D., van Beek, P., Behrens, M.K., Black, E., Bluhm, K., Bopp, L., Bouman, H., Bowman, K., Bown, J., Boyd, P., Boye, M., Boyle, E.A., Branellec, P., Bridgestock, L., Brissebrat, G., Browning, T., Bruland, K.W., Brumsack, H.-J., Brzezinski, M., Buck, C.S., Buck, K.N., Buesseler, K., Bull, A., Butler, E., Cai, P., Mor, P.C., Cardinal, D., Carlson, C., Carrasco, G., Casacuberta, N., Casciotti, K.L., Castrillejo, M., Chamizo, E., Chance, R., Charette, M.A., Chaves, J.E., Cheng, H., Chever, F., Christl, M., Church, T.M., Closset, I., Colman, A., Conway, T.M., Cossa, D., Croot, P., Cullen, J.T., Cutter, G.A., Daniels, C., Dehairs, F., Deng, F., Dieu, H.T., Duggan, B., Dulaquais, G., Dumousseaud, C., Echegoyen-Sanz, Y., Edwards, R.L., Ellwood, M., Fahrbach, E., Fitzsimmons, J.N., Russell Flegal, A., Fleisher, M.Q., van de Flierdt, T., Frank, M., Friedrich, J., Fripiat, F., Fröllje, H., Galer, S.J.G., Gamo, T., Ganeshram, R.S., Garcia-Orellana, J., Garcia-Solsona, E., Gault-Ringold, M., George, E., Gerringa, L.J.A., Gilbert, M., Godoy, J.M., Goldstein, S.L., Gonzalez, S.R., Grissom, K., Hammerschmidt, C., Hartman, A., Hassler, C.S., Hathorne, E.C., Hatta, M., Hawco, N., Hayes, C.T., Heimbürger, L.-E., Helgoe, J., Heller, M., Henderson, G.M., Henderson, P.B., van Heuven, S., Ho, P., Horner, T.J., Hsieh, Y.-T., Huang, K.-F., Humphreys, M.P., Isshiki, K., Jacquot, J.E., Janssen, D.J., Jenkins, W.J., John, S., Jones, E.M., Jones, J.L., Kadko, D.C., Kayser, R., Kenna, T.C., Khondoker, R., Kim, T., Kipp, L., Klar, J.K., Klunder, M., Kretschmer, S., Kumamoto, Y., Laan, P., Labatut, M., Lacan, F., Lam, P.J., Lambelet, M., Lamborg, C.H., Le Moigne, F.A.C., Le Roy, E., Lechtenfeld, O.J., Lee, J.-M., Lherminier, P., Little, S., López-Lora, M., Lu, Y., Masque, P., Mawji, E., Mcclain, C.R., Measures, C., Mehic, S., Barraqueta, J.-L.M., van der Merwe, P., Middag, R., Mieruch, S., Milne, A., Minami, T., Moffett, J.W., Moncoiffe, G., Moore, W.S., Morris, P.J., Morton, P.L., Nakaguchi, Y., Nakayama, N., Niedermiller, J., Nishioka, J., Nishiuchi, A., Noble, A., Obata, H., Ober, S., Ohnemus, D.C., van Ooijen, J., O'Sullivan, J., Owens, S., Pahnke, K., Paul, M., Pavia, F., Pena, L.D., Peters, B., Planchon, F., Planquette, H., Pradoux, C., Puigcorbé, V., Quay, P., Queroue, F., Radic, A., Rauschenberg, S., Rehkämper, M., Rember, R., Remenyi, T., Resing, J.A., Rickli, J., Rigaud, S., Rijkenberg, M.J.A., Rintoul, S., Robinson, L.F., Roca-Martí, M., Rodellas, V., Roeske, T., Rolison, J.M., Rosenberg, M., Roshan,

S., Rutgers van der Loeff, M.M., Ryabenko, E., Saito, M.A., Salt, L.A., Sanial, V., Sarthou, G., Schallenberg, C., Schauer, U., Scher, H., Schlosser, C., Schnetger, B., Scott, P., Sedwick, P.N., Semiletov, I., Shelley, R., Sherrell, R.M., Shiller, A.M., Sigman, D.M., Singh, S.K., Slagter, H.A., Slater, E., Smethie, W.M., Snaith, H., Sohrin, Y., Sohst, B., Sonke, J.E., Speich, S., Steinfeldt, R., Stewart, G., Stichel, T., Stirling, C.H., Stutsman, J., Swarr, G.J., Swift, J.H., Thomas, A., Thorne, K., Till, C.P., Till, R., Townsend, A.T., Townsend, E., Tuerena, R., Twining, B.S., Vance, D., Velazquez, S., Venchiarutti, C., Villa-Alfageme, M., Vivancos, S.M., Voelker, A.H.L., Wake, B., Warner, M.J., Watson, R., van Weerlee, E., Alexandra Weigand, M., Weinstein, Y., Weiss, D., Wisotzki, A., Woodward, E.M.S., Wu, J., Wu, Y., Wuttig, K., Wyatt, N., Xiang, Y., Xie, R.C., Xue, Z., Yoshikawa, H., Zhang, J., Zhang, P., Zhao, Y., Zheng, L., Zheng, X.-Y., Zieringer, M., Zimmer, L.A., Ziveri, P., Zunino, P., Zurbrick, C., 2018. The GEOTRACES Intermediate Data Product 2017. Chem. Geol. https://doi.org/10.1016/j.chemgeo.2018.05.040

Sevilgen, D.S., Venn, A.A., Hu, M.Y., Tambutté, E., de Beer, D., Planas-Bielsa, V., Tambutté, S., 2019. Full in vivo characterization of carbonate chemistry at the site of calcification in corals. Sci. Adv. 5, eaau7447.

Shen, G.T., Boyle, E.A., 1988. Determination of lead, cadmium and other trace metals in annually-banded corals. Chem. Geol. 67, 47–62. https://doi.org/10.1016/0009-2541(88)90005-8

Sieber, M., Conway, T.M., de Souza, G.F., Hassler, C.S., Ellwood, M.J., Vance, D., 2020. Cycling of zinc and its isotopes across multiple zones of the Southern Ocean: Insights from the Antarctic Circumnavigation Expedition. Geochim. Cosmochim. Acta 268, 310–324. https://doi.org/10.1016/j.gca.2019.09.039

Siebert, C., Nägler, T.F., von Blanckenburg, F., Kramers, J.D., 2003. Molybdenum isotope records as a potential new proxy for paleoceanography. Earth Planet. Sci. Lett. 211, 159–171. https://doi.org/10.1016/S0012-821X(03)00189-4

Sigman, D.M., Hain, M.P., Haug, G.H., 2010. The polar ocean and glacial cycles in atmospheric CO2concentration. Nature 466, 47–55. https://doi.org/10.1038/nature09149

Smrzka, D., Zwicker, J., Bach, W., Feng, D., Himmler, T., Chen, D., Peckmann, J., 2019. The behavior of trace elements in seawater, sedimentary pore water, and their incorporation into carbonate minerals: a review. Facies.

https://doi.org/10.1007/s10347-019-0581-4
Sokolov, S., Rintoul, S.R., 2009. Circumpolar structure and distribution of the antarctic circumpolar current fronts: 1. Mean98 circumpolar paths. J. Geophys. Res. Ocean. https://doi.org/10.1029/2008JC005108
Spooner, P.T., Robinson, L.F., Hemsing, F., Morris, P., Stewart, J.A., 2018. Extended calibration of cold-water coral Ba/Ca using multiple genera and co-located measurements of dissolved barium concentration. Chem. Geol. 499, 100–110. https://doi.org/10.1016/j.chemgeo.2018.09.012
Sweere, T.C., Dickson, A.J., Jenkyns, H.C., Porcelli, D., Elrick, M., van den Boorn, S.H.J.M., Henderson, G.M., 2018. Isotopic evidence for changes in the zinc cycle during Oceanic Anoxic Event 2 (Late Cretaceous). Geology 46, 463–466. https://doi.org/10.1130/G40226.1
Takano, S., Tanimizu, M., Hirata, T., Sohrin, Y., 2014. Isotopic constraints on biogeochemical cycling of copper in the ocean. Nat. Commun. 5, 5663. https://doi.org/10.1038/ncomms6663
Temmam, M., Paquette, J., Vali, H., 2000. Mn and Zn incorporation into calcite as a function of chloride aqueous concentration. Geochim. Cosmochim. Acta 64, 2417–2420. https://doi.org/10.1016/S0016-7037(00)00375-6
Thiagarajan, N., Gerlach, D., Roberts, M.L., Burke, A., McNichol, A., Jenkins, W.J., Subhas, A. V., Thresher, R.E., Adkins, J.F., 2013. Movement of deep-sea coral populations on climatic timescales. Paleoceanography 28, 227–236. https://doi.org/10.1002/palo.20023
Thompson, C.M., Ellwood, M.J., 2014. Dissolved copper isotope biogeochemistry in the Tasman Sea, SW Pacific Ocean. Mar. Chem. 165, 1–9. https://doi.org/10.1016/j.marchem.2014.06.009
van de Flierdt, T., Robinson, L.F., Adkins, J.F., 2010. Deep-sea coral aragonite as a recorder for the neodymium isotopic composition of seawater. Geochim. Cosmochim. Acta 74, 6014–6032. https://doi.org/10.1016/j.gca.2010.08.001
van Dijk, I., de Nooijer, L.J., Wolthers, M., Reichart, G.J., 2017. Impacts of pH and [CO32−] on the incorporation of Zn in foraminiferal calcite. Geochim. Cosmochim. Acta 197, 263–277. https://doi.org/10.1016/j.gca.2016.10.031
Vance, D., de Souza, G.F., Zhao, Y., Cullen, J.T., Lohan, M.C., 2019. The relationship between zinc, its isotopes, and the major nutrients in the North-East Pacific. Earth Planet. Sci. Lett. 525, 115748.

https://doi.org/10.1016/j.epsl.2019.115748
Vance, D., Little, S.H., De Souza, G.F., Khatiwala, S., Lohan, M.C., Middag, R., 2017. Silicon and zinc biogeochemical cycles coupled through the Southern Ocean. Nat. Geosci. 10, 202–206. https://doi.org/10.1038/ngeo2890
Veeramani, H., Eagling, J., Jamieson-Hanes, J.H., Kong, L., Ptacek, C.J., Blowes, D.W., 2015. Zinc isotope fractionation as an indicator of geochemical attenuation processes. Environ. Sci. Technol. Lett. 2, 314–319. https://doi.org/10.1021/acs.estlett.5b00273
Wang, R.M., Archer, C., Bowie, A.R., Vance, D., 2018. Zinc and nickel isotopes in seawater from the Indian Sector of the Southern Ocean: The impact of natural iron fertilization versus Southern Ocean hydrography and biogeochemistry. Chem. Geol. 1–13. https://doi.org/10.1016/j.chemgeo.2018.09.010
Weber, T., John, S., Tagliabue, A., DeVries, T., 2018. Biological uptake and reversible scavenging of zinc in the global ocean. Science (80-.). 361, 72–76. https://doi.org/10.1126/science.aap8532
Wilson, D.J., Crocket, K.C., Van De Flierdt, T., Robinson, L.F., Adkins, J.F., 2014. Dynamic intermediate ocean circulation in the North Atlantic during Heinrich Stadial 1: A radiocarbon and neodymium isotope perspective. Paleoceanography 29, 1072–1093. https://doi.org/https://doi.org/10.1002/2014PA002674
Wilson, D.J., van de Flierdt, T., Adkins, J.F., 2017. Lead isotopes in deep-sea coral skeletons: Ground-truthing and a first deglacial Southern Ocean record. Geochim. Cosmochim. Acta 204, 350–374.
Xiao, H., Deng, W., Wei, G., Chen, J., Zheng, X., Shi, T., Chen, X., Wang, C., Liu, X., Zeng, T., 2020. A pilot study on zinc isotopic compositions in shallow-water coral skeletons. Geochemistry, Geophys. Geosystems. https://doi.org/10.1029/2020gc009430
Yu, J., Elderfield, H., Greaves, M., Day, J., 2007. Preferential dissolution of benthic foraminiferal calcite during laboratory reductive cleaning. Geochemistry, Geophys. Geosystems 8. https://doi.org/10.1029/2006GC001571
Zhao, M., Tarhan, L.G., Zhang, Y., Hood, A., Asael, D., Reid, R.P., Planavsky, N.J., 2021. Evaluation of shallow-water carbonates as a seawater zinc isotope archive. Earth Planet. Sci. Lett. 553, 116599. https://doi.org/https://doi.org/10.1016/j.epsl.2020.116599
Zhao, Y., Vance, D., Abouchami, W., de Baar, H.J.W., 2014. Biogeochemical cycling

of zinc and its isotopes in the Southern Ocean. Geochim. Cosmochim. Acta 125, 653–672. https://doi.org/10.1016/j.gca.2013.07.045

Table 1. Location, taxonomic classification, water depth and water mass, and age of cold-water coral specimens included in this study

Table 1A: Holocene age coral specimens

Study ID	Locality	Full ID	Genus	species	Depth (m)	Age (yr)	Modern water mass	Latitude (°N)	Longitude (°E)
Iceland									
1	Reykjanes Ridge	CE0806 D19A #2	*Desmophyllum*	*dianthus*	1545	Modern	ISOW/LSW	58.8	-32.0
2	Reykjanes Ridge	CE0806 D19A #1B	*Desmophyllum*	*dianthus*	1545	Modern	ISOW/LSW	58.8	-32.0
2 Coat	Iceland - Reykjanes Ridge	CE0806 D19A #1B	coating						
Drake Passage									
3	Burdwood Bank	NBP0805 TB04 "Big Beauty"	*Desmophyllum*	*dianthus*	816	468	AAIW	-54.4	-62.1
4	Burdwood Bank	NBP1103 DH14 Cn7	*Caryophyllia*	*sp.*	727	1170	SAMW	-54.7	-62.2
5	Sars Seamount	NBP1103 DH95 Dc7	*Desmophyllum*	*dianthus*	776	434	UCDW	-59.7	-68.9
5 Coat	Sars Seamount	NBP1103 DH95 Dc7	uncleaned coral						
6	Sars Seamount	NBP1103 DH97 Dp1	*Desmophyllum*	*dianthus*	658	281	UCDW	-59.7	-68.9
7	Sars Seamount	NBP1103 DH97 CC1	*Caryophyllia*	*sp.*	658	346	UCDW	-59.7	-68.9
7 Coat	Sars Seamount	NBP1103 DH97 CC1	coating						
Eastern Equatorial Atlantic									
8	Carter Seamount	JC094 BO244 Carls 001	*Caryophyllia*	*sp.*	621	Modern	AAIW*	9.2	-21.3
9	Carter Seamount	JC094 BO712 Carlm 001	*Caryophyllia*	*sp.*	2260	Modern	NADW	9.2	-21.3
10	Carter Seamount	JC094 BO424 Das ls/m 002	*Dasmosmilia*	*sp.*	265	Modern	STMW	9.2	-21.3
11	Carter Seamount	JC094 BO457 Daslm 001	*Dasmosmilia*	*sp.*	321	Modern	STMW	9.2	-21.3
Southwest Indian Ocean									
13	Melville Bank	JC066-3245	*Caryophyllia*	*profunda*	171.9	841	STSW	-38.5	48.7
15	Coral Seamount	JC066-117	*Desmophyllum*	*dianthus*	1207.2	1476	UCDW	-41.3	42.9
15 Coat	Coral Seamount	JC066-117	coating						
14	Atlantis Bank	JC066-3697	*Caryophyllia*	*diomedeae*	823	200	SAMW	-32.7	57.3
16	Atlantis Bank	JC066-3718	*Desmophyllum*	*dianthus*	1035	166	AAIW*	-32.7	57.2
22	Atlantis Bank	JC066-3661	*Caryophyllia*	*laevigata*	743	762	SAMW	-32.7	57.2
23	Atlantis Bank	JC066-3705	*Caryophyllia*	*diomedeae*	870	965	SAMW	-32.7	57.2
Northwest Atlantic									
17	Manning Seamount	ALV-3883-1248-003-003	*Desmophyllum*	*dianthus*	1524	118	NADW	38.2	-60.5
Tasman Sea									
19	Tasmania (S Hills - Shelf)	TN228-J2-387-1225-1253-11-1898-003	*Desmophyllum*	*dianthus*	1898	113	UCDW	*-44.4*	*147.3*
21	Tasmania (E of St Helens - East)	TN228-J2-389-0101-0930-07-1296-001	*Desmophyllum*	*dianthus*	1296	521	UCDW	*-41.5*	*148.5*

Table 1B: Glacial age coral specimens

Study ID	Locality	Full ID	Genus	species	Depth (m)	Age (yr)	Modern water mass	Latitude (°N)	Longitude (°E)
18	NW Atlantic, Muir Seamount	ALV-3885-1325-002-034	*Desmophyllum*	*dianthus*	1986	48939	NADW	33.8	-62.5
18 Coat	NW Atlantic, Muir Seamount	ALV-3885-1325-002-034	coating						
20	Carter Seamount	JC094-F00001-Descm-008	*Desmophyllum*	*dianthus*	1080	14580	AAIW/NADW	9.2	-21.3
20 Coat	Carter Seamount	JC094-F00001-Descm-008	coating						
DC-01	Sars Seamount	NBP1103 DH115 DC-01	*Desmophyllum*	*dianthus*	843	28184	UCDW	-59.7	-68.9
DC Coat	Sars Seamount	NBP1103 DH115 DC-01	coating						
SS0108	Tasmania	SS0108	*Desmophyllum*	*dianthus*	1200	73510	UCDW	*-44.1*	*147.1*
SS Coat	Tasmania	SS0108	coating						

References:

Burke (2012)	Iceland	^{14}C
Margolin et al. (2014)	Drake Passage	U-series
Chen et al. (2016)	Equatorial Atlantic	U-series
Pratt et al. (2019)	Southwest Indian Ocean	U-series
Robinson et al. (2007)	Northwest Atlantic	U-series
Thiagarajan et al. (2013)	Tasman Sea	^{14}C

DC-01 and SS0108: Cleaning specimens; see Table 2.

Lat/Long in italics: estimated

Table 2. Cleaning experiment results for two *D. dianthus* corals with well-developed coatings: DH115-DC-01 from the Drake Passage, and SS0108 from Tasmania. Trace element/Ca ratios (from ICP-MS, except Zn[$]), Zn and Cu concentrations and isotope compositions.

Sample ID	Li/Ca µmol/mol	Na/Ca mmol/mol	Mg/Ca mmol/mol	Al/Ca µmol/mol	Mn/Ca µmol/mol	Fe/Ca µmol/mol	Cu/Ca µmol/mol	Zn/Ca[$] µmol/mol	Sr/Ca mmol/mol	Cd/Ca µmol/mol	Ba/Ca µmol/mol	U/Ca nmol/mol	Zn[$] µg/g	δ^{66}Zn ‰	2SE	Cu µg/g	δ^{65}Cu ‰	2SE
DH115-DC-01, Drake Passage																		
DC-Coat	18.6	39.5	7.68	2646	13840	20206	51.6	244.5	sat	0.94	142.7	3544	146.1	0.55	0.05	60.30	-0.01	0.04
UNCL	12.1	17.0	1.78	156	496	868	6.27	3.26	sat	0.50	26.1	2686	3.26	0.70	0.05	3.41	0.13	0.04
PHYS-1	9.6	17.8	1.69	bd	0.38	2.38	0.51	0.90	sat	0.58	14.0	2607	0.90	0.46	0.05	0.33		
PHYS-2	9.6	17.4	1.60	bd	0.34	1.67	0.45	0.37	sat	0.55	14.8	2862	0.37	0.40	0.05	0.28	0.78	0.04
PHYS-3	9.8	17.4	1.64	bd	0.22	1.30	0.44	0.58	sat	0.54	14.2	2686	0.58	0.46	0.07	0.33		
PHYS-4	9.0	17.5	1.62	bd	1.00	1.55	0.80	0.42	13.2	0.60	15.2	2938	0.42	0.41	0.04	0.46	0.85	0.04
OXIC-1	10.0	17.5	1.60	bd	0.71	2.83	0.74	0.38	sat	0.55	14.2	2753	0.38	0.46	0.04	0.48	0.68	0.05
OXIC-2	11.3	18.0	1.79	bd	0.25	3.23	0.49	0.84	sat	0.57	14.1	2561	0.84	0.36	0.03	0.32		
OXIC-3	10.8	17.5	1.57	bd	0.56	2.20	0.58	0.37	sat	0.56	15.2	3025	0.37	0.44	0.04	0.36		
OXIC-4	9.1	17.4	1.57	bd	0.45	1.92	0.52	0.48	13.4	0.59	15.2	3059	0.48	0.40	0.03	0.29	0.89	0.03
FULL-1	8.7	17.0	1.54	bd	0.12	0.66	0.38	0.68	sat	0.56	14.3	2717	0.68	0.39	0.04	0.25		
FULL-2	9.1	17.1	1.50	bd	0.07	1.01	0.37	0.43	sat	0.53	13.9	2890	0.43	0.36	0.04	0.22		
FULL-3	10.8	17.9	1.75	2.2	1.23	5.18	0.67	0.57	sat	0.57	14.3	2624	0.57	0.40	0.04	0.34	0.84	0.04
FULL-4	9.0	17.7	1.61	bd	0.12	1.06	0.48	0.38	13.0	0.59	14.6	2950	0.38	0.39	0.03	0.27	0.85	0.05
SS0108, Tasmania																		
SS-Coat	24.4	43.7	9.93	2457	1805	3640	20.6	28.5	11.9	1.15	65.6	2430	18.6	0.25	0.05	8.22	0.23	0.02
UNCL-1	11.1	17.3	1.94	358	64	272	2.94	1.94	12.7	0.94	16.4	2086	1.27	0.26	0.06	0.93	0.38	0.03
UNCL-2	10.7	17.0	2.00	247	30	164	2.52	1.35	12.5	0.95	15.2	2162	0.88	0.22	0.05	1.60	0.30	0.03
UNCL-3	11.9	17.4	1.99	441	51	344	4.25	2.49	12.8	1.03	17.5	2220	1.63	0.22	0.03	1.35	0.34	0.04
PHYS-1	9.6	17.3	1.88	24	0.89	20.0	1.44	0.62	12.8	0.99	14.4	1977	0.44	0.38	0.06	0.97	0.51	0.03
PHYS-3	9.8	17.6	1.93	34	1.43	21.9	1.63		12.6	1.02	14.5	1978						
PHYS-2	10.2	17.4	1.88	33	4.64	22.4	1.85	0.62	12.6	1.03	14.3	1984	0.32	0.27	0.05	1.18	0.39	0.02
OXIC-1	9.7	17.7	1.90	16	0.90	10.7	1.36	0.50	12.3	0.98	14.0	1881	0.33	-		0.86	0.54	0.02
OXIC-2	11.7	18.6	2.23	38	1.51	44.6	2.96	0.71	12.8	1.06	15.7	1883	0.46	0.39	0.04	1.56	0.43	0.03
OXIC-3	10.0	17.8	1.86	42	0.99	30.1	1.90		12.5	1.04	14.5	2001						
OXIC-4	10.6	17.6	1.98	13	0.62	12.3	1.24	0.48	sat	0.99	13.9	1831	0.31	0.45	0.05	0.79	0.46	0.05
FULL-1	9.6	18.1	1.85	18	0.42	14.4	0.61		12.4	1.03	13.9	1834						
FULL-2	9.5	18.0	1.85	15	0.44	9.4	0.58	0.50	12.5	1.03	14.1	1933	0.33	0.40	0.04	0.35	0.75	0.03
FULL-3	10.0	17.9	1.80	19	0.31	13.5	0.44		12.4	1.04	14.2	1822						
FULL-4	10.4	18.0	1.93	13	0.31	15.7	0.58	0.51	Sat	0.98	13.6	1828	0.33	0.34	0.05	0.39		

See main text for description of sample ID codes (Coat, UNCL, PHYS, OXIC, FULL)
bd: Al concentrations below detection limit, where detection limit estimated at 3*blank

sat: > 10^9 counts Sr during Element analysis
[$]Zn concentrations calculated by isotope dilution (Ca concentration for Zn/Ca calculated based on coral mass and molecular mass of $CaCO_3$). N.B. Excludes Zn/Ca ratios of coatings, which are from Element ICP-MS
Merged aliquots for isotope analysis on Tasmania coral (SS0108) samples: PHYS-1 and PHYS-3; OXIC-2 and OXIC-3; FULL-1, FULL-2, and FULL-3
External 2SD on $\delta^{66}Zn$ = 0.07‰, and on $\delta^{65}Cu$ = 0.11‰ (based on repeat analyses of secondary carbonate standard)

Table 3. Trace element/Ca ratios of cold-water corals

Table 3A: Holocene age coral specimens

Sample ID[+]	Locality	Species	Depth (m)	Age (yr)	Li/Ca µmol/mol	Na/Ca mmol/mol	Mg/Ca mmol/mol	Al/Ca µmol/mol	Mn/Ca µmol/mol	Fe/Ca µmol/mol	Cu/Ca µmol/mol	Zn/Ca[$] µmol/mol	Sr/Ca mmol/mol	Cd/Ca µmol/mol	Ba/Ca µmol/mol	U/Ca nmol/mol
Iceland																
1A	Reykjanes Ridge	*D. dianthus*	1545	Modern	15.0	23.2	3.63	bd	0.15	0.83	0.38	0.42	13.1	0.06	8.0	1166
1B					13.7	22.5	3.37	bd	0.06	1.25	0.29	-	12.5	0.05	7.5	1189
1C					14.9	23.4	3.70	bd	0.28	0.91	0.47	0.77	12.5	0.06	7.7	1117
2A	Reykjanes Ridge	*D. dianthus*	1545	Modern	13.3	22.5	3.42	bd	0.23	0.90	0.45	2.90	12.6	0.06	7.7	1193
2B					12.5	21.6	3.19	bd	0.21	0.81	0.27	3.07	12.4	0.06	7.5	1194
2 Coat		Coating			11.9	31.6	8.58	306	92	1753	19.9	54.4	12.4	0.88	9.6	1636
Drake Passage																
3A	Burdwood Bank	*D. dianthus*	816	468	8.2	18.7	2.01	bd	0.08	0.86	0.20	1.20	12.8	0.12	12.4	2218
3B					8.5	19.2	2.11	bd	0.12	1.03	0.22	1.43	12.9	0.12	12.5	2205
3C					9.4	19.1	2.23	bd	0.29	0.81	0.17	-	12.8	0.13	11.9	1993
4A	Burdwood Bank	*Caryophyllia*	727	1170	8.4	17.2	1.95	bd	0.14	0.19	0.13	0.86	12.8	0.34	12.0	1674
4B					nd											
5A	Sars Seamount	*D. dianthus*	776	434	10.5	20.0	2.62	bd	0.07	0.49	0.23	2.24	12.8	0.60	14.7	1754
5B					10.7	19.8	2.59	bd	0.04	1.03	0.18	-	13.0	0.58	14.1	1659
5D					12.7	20.7	3.12	bd	0.02	0.69	0.11	2.93	12.9	0.54	14.2	1414
5 Coat		Unclean coral			11.1	29.4	5.45	2208	109	1918	3.80	4.80	12.6	0.60	22.7	2074
6A	Sars Seamount	*D. dianthus*	658	281	10.7	20.2	2.71	bd	0.16	0.72	0.25	1.43	13.2	0.79	14.5	1840
6B					11.1	20.2	2.90	2.6	0.08	0.51	0.19	-	12.9	0.72	13.8	1734
7	Sars Seamount	*Caryophyllia*	658	346	11.7	20.7	2.77	3.1	0.26	0.32	0.47	9.33	13.1	0.17	16.2	1760
7 Coat		Coating			9.8	31.4	6.60	323	3704	2483	15.9	27.0	13.3	0.43	39.1	2464
Eastern Equatorial Atlantic																
8A	Carter Seamount	*Caryophyllia*	621	Modern	8.8	19.7	2.49	bd	0.48	3.40	0.77	12.4	12.3	1.59	10.3	1758
8B					9.8	20.2	2.73	bd	0.41	3.70	0.76	12.7	12.2	1.31	10.2	1565
9	Carter Seamount	*Caryophyllia*	2260	Modern	7.9	15.9	1.65	bd	0.16	0.25	0.13	2.99	12.3	0.37	10.3	1771
10	Carter Seamount	*Dasmosmilia*	265	Modern	10.4	23.7	3.59	bd	0.25	0.35	0.34	2.18	12.4	0.15	8.0	1102
11A	Carter Seamount	*Dasmosmilia*	321	Modern	10.2	22.8	3.34	bd	0.20	0.67	0.21	0.49	12.4	0.20	8.3	1256
11B					8.8	17.2	1.90	bd	0.20	0.20	0.11	-	12.7	0.37	10.1	1658
Southwest Indian Ocean																
13	Melville Bank	*C. profunda*	172	841	8.9	18.5	2.41	bd	0.47	0.26	0.32	2.15	12.9	0.73	14.2	1820
15	Coral Seamount	*D. dianthus*	1207	1476	9.8	19.5	2.13	bd	0.18	2.20	0.21	1.87	12.9	0.16	15.1	2182

15 Coat		Coating			17.1	46.4	8.07	1207	2931	2105	15.7	54.1	11.8	0.36	50.4	2037
14	Atlantis Bank	*C. diomedeae*	823	200	11.3	21.8	3.31	bd	0.38	2.89	0.37	2.56	12.2	1.25	8.4	1316
16A	Atlantis Bank	*D. dianthus*	1035	166	13.4	22.5	4.32	bd	0.21	1.87	0.16	1.04	12.2	0.13	10.2	1349
16B					13.9	23.2	4.57	bd	0.16	2.50	0.15	0.84	12.5	0.12	10.3	1286
22	Atlantis Bank	*C. laevigata*	743	762	10.8	21.7	3.50	bd	0.16	1.59	0.80	5.87	12.6	0.76	7.8	1400
23	Atlantis Bank	*C. diomedeae*	870	965	9.9	20.4	3.15	bd	0.06	1.21	0.78	16.8	12.2	1.91	8.6	1451
Northwest Atlantic																
17A*	Manning Seamount	D. dianthus	1524	118	10.8	20.3	2.59	14.7	0.13	6.68	0.16	0.52	12.0	0.08	8.3	1410
17B*					11.5	21.0	2.82	28.5	0.50	15.2	0.22	0.58	12.4	0.10	8.8	1410
Tasman Sea																
19	South Hills - Shelf	*D. dianthus*	1898	113	8.3	18.2	1.96	bd	0.07	2.47	0.31	2.24	12.0	0.43	14.8	1969
21	East of St Helens	*D. dianthus*	1296	521	11.7	20.0	3.42	1.6	0.34	1.58	1.00	2.63	12.4	0.11	15.3	1753

Table 3B: Glacial age coral specimens

Sample ID[+]	Locality	Species	Depth (m)	Age (yr)	Li/Ca µmol/mol	Na/Ca mmol/mol	Mg/Ca mmol/mol	Al/Ca µmol/mol	Mn/Ca µmol/mol	Fe/Ca µmol/mol	Cu/Ca µmol/mol	Zn/Ca[$] µmol/mol	Sr/Ca mmol/mol	Cd/Ca µmol/mol	Ba/Ca µmol/mol	U/Ca nmol/mol
18A	NW Atlantic, Muir Seamount	*D. dianthus*	1986	48939	12.4	18.8	2.36	4.9	0.12	4.53	0.27	2.39	12.3	0.28	13.5	1445
18B					11.6	18.7	2.28	bd	0.07	2.31	0.24	3.02	12.2	0.31	13.3	1537
18 Coat		Coating			132	181	135	38404	367896	442651	424	1035	9.5	4.20	923	10508
20	Equat. Atlantic, Carter Seamount	*D. dianthus*	1080	14580	8.3	18.2	1.99	7.8	1.18	5.65	0.16	0.65	12.5	0.25	11.8	2011
20 Coat		Coating			46.5	27.5	9.74	10005	5422	18053	18.7	37.0	10.9	0.91	59.5	2337
SS	Tasman Sea	*D. dianthus*	1200	73510	9.9	18.0	1.86	16.1	0.37	13.3	0.55	0.50	12.4	1.02	14.0	1854
SS Coat		Coating			24.4	43.7	9.93	2457	1805	3640	20.6	28.5	11.9	1.15	65.6	2430
DC	Drake Passage, Sars Seamount	*D. dianthus*	843	28184	9.4	17.4	1.60	bd	0.38	1.98	0.47	0.52	13.0	0.56	14.3	2795
DC Coat		Coating			18.6	39.5	7.68	2646	13840	20206	51.6	244	sat	0.94	143	3544

bd: Al concentrations below detection limit, where detection limit estimated at 3 × blank

[+]Letters after sample numbers (A-D) indicate full replicate sub-samples

[$]Zn concentrations calculated by isotope dilution (Ca concentration calculated based on coral mass and molecular mass of $CaCO_3$). N.B. Excludes Zn/Ca ratios of coatings, which are from Element ICP-MS. All other Me/Ca ratios from ICP-MS.

*Sample 17 (particularly sub-sample 17B) remained visibly unclean after physical cleaning

Table 4. Cold-water coral Zn/Ca and Cu/Ca ratios, calculated partition coefficients D_{Zn} and D_{Cu}, and Zn and Cu isotope compositions. Also given are estimates of ambient seawater Zn and Cu concentrations and $\delta^{66}Zn$ values

Table 4A: Holocene age coral specimens

					Coral Zn			Ambient seawater Zn				Coral Cu			Ambient seawater Cu	
Sample ID	Locality	Species	Depth (m)	Age (yr)	Zn/Ca[$] µmol/mol	D_{Zn}	$\delta^{66}Zn$ ‰ ± 2SE	Estimated [Zn] nmol/kg	Ref	Estimated $\delta^{66}Zn$ ‰, 1SD (range)	Ref	Cu/Ca µmol/mol	D_{Cu}	$\delta^{65}Cu$ ‰ ± 2SE	Estimated [Cu] nmol/kg	Ref
Iceland																
1A	Reykjanes Ridge	*D. dianthus*	1545	Modern	0.42	(1.0 to) 4.4	+0.67 ± 0.05	1.4 (to 6.0)	a	+0.47 ± 0.06 (-0.2 to +0.5)	a	0.38	2.8	-	1.4 ± 0.2	IDP17
1B					-		-					0.29		+0.45 ± 0.05		
1C					0.77		+0.55 ± 0.03					0.47		+0.25 ± 0.06		
2A	Reykjanes Ridge	*D. dianthus*	1545	Modern	2.90	(5.1 to) 22	+0.68 ± 0.04	1.4 (to 6.0)	a	+0.47 ± 0.06 (-0.2 to +0.5)	a	0.45	3.3	+0.76 ± 0.06	1.4 ± 0.2	IDP17
2B					3.07		+0.64, +0.59					0.27		-		
2 Coat		Coating			54.4		+0.37 ± 0.04					19.9		+0.26 ± 0.04		
Drake Passage																
3A	Burdwood Bank, N of SAF	*D. dianthus*	816	468	1.20	4.4	+0.37 ± 0.03	3.1 ± 0.6	b	+0.42 ± 0.08	b	0.20	1.3	-	1.3 ± 0.2	f
3B					1.43		+0.37, +0.41					0.22		-		
3C					-		-					0.17		+0.32 ± 0.13		
4A	Burdwood Bank	*Caryophyllia*	727	1170	0.86	3.1	+0.36 ± 0.03	2.8 ± 0.3	b	+0.42 ± 0.08	b	0.13	1.1	-	1.2 ± 0.2	f
4B					-		-					nd		+0.55 ± 0.16		
5A	Sars Seamount, between PF and SAF	*D. dianthus*	776	434	2.24	4.5	+0.39 ± 0.03	5.9 ± 0.3	c	+0.39 ± 0.04	c	0.23	1.0	-	1.85 ± 0.1	f
5B					-		-					0.18		+0.76 ± 0.10		
5D					2.93		+0.32 ± 0.04					0.11		-		
5 Coat		Unclean coral			4.80		+0.58 ± 0.05					3.80		+0.11 ± 0.04		
6A	Sars Seamount	*D. dianthus*	658	281	1.43	2.6	+0.33, +0.35	5.7 ± 0.3	c	+0.39 ± 0.04	c	0.25	1.1	-	1.8 ± 0.1	f
6B					-		-					0.19		+0.85 ± 0.10		
7	Sars Seamount	*Caryophyllia*	658	346	9.33	17	+0.44 ± 0.04	5.7 ± 0.3	c	+0.39 ± 0.04	c	0.47	2.7	-	1.8 ± 0.1	f
7 Coat		Coating			27.0		+0.61 ± 0.04					15.9		+0.18 ± 0.05		
Eastern Equatorial Atlantic																
8A	Carter Seamount	*Caryophyllia*	621	Modern	12.4	92	+0.35 ± 0.04	1.4 ± 0.2	d	+0.33 ± 0.14	d	0.77	7.2	-	1.1 ± 0.1	g
8B					12.7		+0.30, +0.33					0.76		-		
9	Carter Seamount	*Caryophyllia*	2260	Modern	2.99	18	+0.63 ± 0.03	1.7 ± 0.2	d	+0.59 ± 0.04	d	0.13	0.9	-	1.5 ± 0.1	g
10	Carter Seamount	*Dasmosmilia*	265	Modern	2.18	45	+0.64 ± 0.04	0.5 ± 0.2	d	+0.18 ± 0.18	d	0.34	3.8	-	0.9 ± 0.1	g
11A	Carter Seamount	*Dasmosmilia*	321	Modern	0.49	8.4	+0.57 ± 0.04	0.6 ± 0.2	d	+0.42 ± 0.08	d	0.21	1.2	-	0.9 ± 0.1	g
11B					-		-					0.11		+0.95 ± 0.12		

Southwest Indian Ocean																
13	Melville Bank	*C. profunda*	171.9	841	2.15	25	+0.60 ± 0.04	0.9 ± 0.2	IDP17	*+0.4 ± 0.2*	x	0.32	4.6	+0.27 ± 0.05	0.7 ± 0.2	IDP17
15	Coral Seamount	*D. dianthus*	1207.2	1476	1.87	5.1	+0.58 ± 0.03	3.8 ± 0.6	IDP17	+0.42 ± 0.08	b	0.21	2.4	+0.44 ± 0.05	0.9 ± 0.1	IDP17
15 Coat		Coating			54.1		+0.60 ± 0.03					15.7		+0.26 ± 0.05		
14	Atlantis Bank	*C. diomedeae*	823	200	2.56	18	+0.07 ± 0.03	1.5 ± 0.3	IDP17	+0.42 ± 0.08	b	0.37	4.4	+0.50 ± 0.05	0.85 ± 0.1	IDP17
16A	Atlantis Bank	*D. dianthus*	1035	166	1.04	4.0	+0.39 ± 0.04	2.4 ± 0.3	IDP17	+0.42 ± 0.08	b	0.16	1.7	+0.59 ± 0.07	0.95 ± 0.1	IDP17
16B					0.84		+0.48 ± 0.03					0.15		+0.68 ± 0.09		
22	Atlantis Bank	*C. laevigata*	743	762	5.87	43	+0.29 ± 0.04	1.4 ± 0.3	IDP17	+0.42 ± 0.08	b	0.80	10.3	+0.59 ± 0.05	0.8 ± 0.1	IDP17
23	Atlantis Bank	*C. diomedeae*	870	965	16.8	91	+0.39 ± 0.04	1.9 ± 0.3	IDP17	+0.42 ± 0.08	b	0.78	8.9	+1.05 ± 0.09	0.9 ± 0.1	IDP17
Northwest Atlantic																
*17A**	Manning Seamount	*D. dianthus*	1524	118	*0.52*	*3.8*	*+0.61 ± 0.04*	1.5 ± 0.2	d	+0.46 ± 0.04	d	*0.16*	*1.2*	*+0.62 ± 0.07*	1.35 ± 0.1	g
*17B**					*0.58*		*+0.54 ± 0.04*					*0.22*		*+0.54 ± 0.04*		
Tasman Sea																
19	South Hills - Shelf	*D. dianthus*	1898	113	2.24	4.4	+0.29 ± 0.04	5.3 ± 0.3	e	+0.48 ± 0.05	e	0.31	1.6	+0.54 ± 0.04	2.0 ± 0.1	h
21	East of St Helens	*D. dianthus*	1296	521	2.63	6.5	+0.48 ± 0.03	4.2 ± 0.6	e	+0.51 ± 0.07	e	1.00	6.4	+0.30 ± 0.05	1.6 ± 0.1	h

Table 4B: Glacial age coral specimens

Sample ID	Locality	Species	Depth (m)	Age (yr)	Coral Zn		Coral Cu	
					Zn/Ca[$]	δ^{66}Zn	Cu/Ca	δ^{65}Cu
					µmol/mol	‰ ± 2SE	µmol/mol	‰ ± 2SE
18A	NW Atlantic, Muir Seamount	*D. dianthus*	1986	48939	2.39	+0.66 ± 0.03	0.27	+0.69 ± 0.05
18B					3.02	+0.68 ± 0.03	0.24	+0.62 ± 0.06
18 Coat		Coating			1035	+0.90 ± 0.03	424	0.00 ± 0.03
20	Carter Seamount	*D. dianthus*	1080	14580	0.65	+0.79 ± 0.04	0.16	+0.70 ± 0.07
20 Coat		Coating			37.0	+0.51 ± 0.04	19	+0.22 ± 0.04
SS	Tasman Sea	*D. dianthus*	1200	73510	0.50	+0.37 ± 0.04	0.55	+0.73 ± 0.04
SS Coat		Coating			28.5	+0.25 ± 0.05	20.6	+0.23 ± 0.02
DC	Sars Seamount	*D. dianthus*	843	28184	0.52	+0.38 ± 0.04	0.47	+0.84 ± 0.02
DC Coat		Coating			244	+0.55 ± 0.05	51.6	-0.01 ± 0.04

[$]Zn concentrations calculated by isotope dilution (Ca concentration calculated based on coral mass and molecular mass of $CaCO_3$). N.B. Excludes Zn/Ca ratios of coatings, which are from Element ICP-MS. All other Me/Ca ratios from ICP-MS.
Two Zn isotope values for the same sub-sample indicate reanalysis of the sub-sample after a third Zn clean-up column
*Sample 17 (particularly sub-sample 17B) remained visibly unclean after physical cleaning
External 2SD on δ^{66}Zn = 0.07‰, and on δ^{65}Cu = 0.11‰ (based on repeat analyses of secondary carbonate standard)
Error bars on figures are the external 2SD, except where the internal 2SE is larger (for samples with low Cu contents)

References:
a. Lemaitre et al., 2020, GEOVIDE stations 32, 38, 44 (values in brackets indicate hydrothermal influence inferred by those authors)
b. Southern Ocean > 200m, mean of all data from Sieber et al. 2020 and Wang et al., 2019
c. Sieber et al., 2020, ACE station 20
d. Conway and John, 2014. Carter: USGT10-11 and 10-10. Manning: USGT11-8, 11-10
e. Samanta et al., 2017, Tasman Sea stations P2 and P3
f. Heller and Croot, 2015, stations 249, 236
g. Roshan and Wu, 2015, USGT10-11, USGT11-10
h. Thompson et al., 2014, Tasman Sea station P3
x. Surface ocean estimate for Melville Bank coral based on approximate range of deep water $\delta^{66}Zn$ values
IDP17: Schlitzer et al., 2019